ANALOG SINGLE SIDEBAND-PULSE WIDTH MODULATION PROCESSOR FOR PARAMETRIC ACOUSTIC ARRAYS

A Thesis

presented to

the Faculty of California Polytechnic State University,

San Luis Obispo

In Partial Fulfillment

of the Requirements for the Degree

Master of Science in Electrical Engineering

by

Vikrant A. Marathe

June 2019

COMMITTEE MEMBERSHIP

TITLE: Analog Single Sideband-Pulse Width Modulation Processor for Parametric Acoustic Arrays

AUTHOR: Vikrant A. Marathe

DATE SUBMITTED: June 2019

COMMITTEE CHAIR: Vladimir Prodanov, Ph.D.
Associate Professor of Electrical Engineering

COMMITTEE MEMBER: Wayne Pilkington, Ph.D.
Associate Professor of Electrical Engineering

COMMITTEE MEMBER: Tina Smilkstein, Ph.D.
Associate Professor of Electrical Engineering

ABSTRACT

Analog Single Sideband-Pulse Width Modulation Processor for Parametric Acoustic Arrays

Vikrant A. Marathe

Parametric acoustic arrays are ultrasonic-based loudspeakers that produce highly directive audio. The audio must first be preprocessed and modulated into an ultrasonic carrier before being emitted into the air, where it will self-demodulate in the far field. The resulting audio wave is proportional to the double time-derivative of the square of the modulation envelope. This thesis presents a fully analog processor which encodes the audio into two Pulse Width Modulated (PWM) signals in quadrature phase and sums them together to produce a Single Sideband (SSB) spectrum around the fundamental frequency of the PWM signals. The two signals are modulated between 8% and 24% duty cycle to maintain a quasi-linear relationship between the duty cycle and the output signal level. This also allows the signals to sum without overlapping each other, maintaining a two-level output. The system drives a network of narrowband transducers with a center frequency equal to the PWM fundamental. Because the transducers are voltage driven, they have a bandpass frequency response which behaves as a first-order integrator on the SSB signal, eliminating the need for two integrators in the processor. Results show that the “SSB-PWM” output wave has a consistent 20-30dB difference in magnitude between the upper sideband and lower sideband. In simulation, a single tone test shows higher total harmonic distortion for lower frequencies and higher modulation depth. A two-tone test creates a 2_{nd} order intermodulation term that increases with the frequencies of the input signals.

Keywords: parametric loudspeaker, Berktay’s equation, amplitude modulation, bandpass PWM, polyphase networks, Hilbert transform, monostable multivibrator, series resonance

ACKNOWLEDGMENTS

Thank you Dr. Prodanov for providing assistance, advice and resources throughout the duration of the project. Thank you also to Dr Pilkington and Dr. Smilkstein for sitting on the committee.

TABLE OF CONTENTS

Page

LIST OF TABLES

Table Page

LIST OF FIGURES

Figure Page

Chapter 1

INTRODUCTION

1.1 Parametric Acoustic Arrays

Parametric acoustic arrays or parametric loudspeakers are ultrasound-based loudspeakers featuring a highly directive output audio field, minimal sidelobe content, and a small aperture size relative to traditional speakers [1]. They consist of three main segments: a signal preprocessing block which conditions and modulates an ultrasonic carrier signal with an audio signal, an amplifier/driver which boosts the signal to an appropriate level, and a network of ultrasonic transducers which emit the output signal as mechanical waves. When an amplitude modulated ultrasonic wave travels through a nonlinear medium such as air, the wave self demodulates and produces a distorted version of the baseband audio signal, creating the effect of a “virtual source” in the air. Figure 1 is a simple visualization of this process. The high frequency wave that is first emitted is the primary beam, and the demodulated wave is the secondary beam.

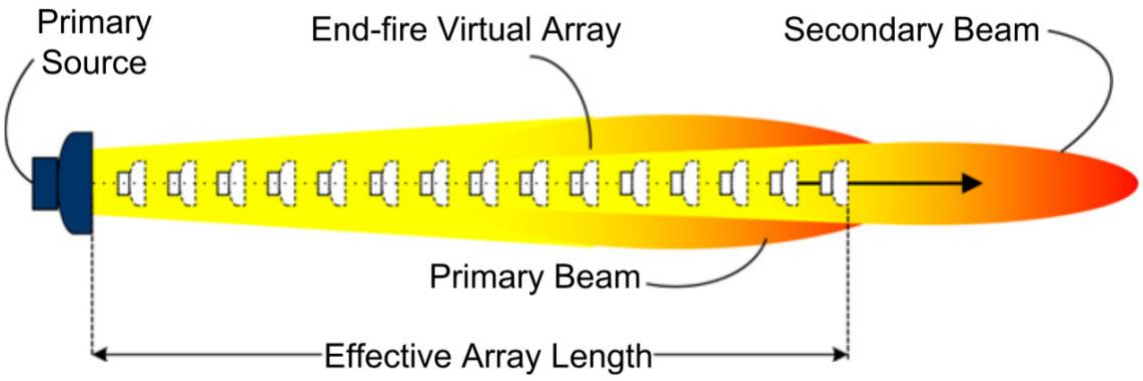

Figure 1: Visualization of Parametric Loudspeaker Producing Audio (2012_Gan, Yang, and Kamakura)

Many improvements have been made to reduce distortion in the output audio, such as the use of equalizers and alternative modulation [2] schemes in the preprocessing segment. Larger bandwidth [7] ultrasonic transducers also improve sound quality with a flatter frequency response.

1.2 Thesis Statements

This thesis will present a new design choice for parametric arrays that generates a summation of two low duty cycle Pulse Width Modulated (PWM) waveforms and drives a narrowband transducer array with a center frequency equal to the PWM fundamental frequency. The idea is to utilize the energy surrounding the PWM fundamental frequency, which has a spectrum that resembles a Single Sideband Amplitude Modulated signal (SSB-AM). Unlike normal AM however, the dual PWM signal only has two levels, allowing for the use of a switching amplifier instead of a linear amplifier. The low duty cycle range (0-25%) keeps a fairly linear relationship between the input audio signal and the PWM fundamental frequency magnitude. It also takes advantage of the narrowband frequency response of inexpensive ultrasonic transmitters, which behave like a first order integrator to equalize the sideband spectrum.

The ultimate goal is to produce audio from the analog SSB-PWM parametric array and analyze the output for total harmonic distortion. The signal distortion can be compared to that of previous renditions of the system to determine if there is an overall improvement or not.

1.3 Organization of Thesis

After the introductory chapter, the paper will be organized in the following manner. Chapter 2 provides the background information necessary for the reader to understand the system design. This includes a brief theory behind parametric loudspeakers, some of the previous design choices, and other important concepts related to the design such as SSB-AM. Chapter 3 details any preliminary work that was done prior to building the system. Chapter 4 examines the system design both as a whole and on a subsystem to subsystem basis. Chapter 5 discusses the testing schemes both in simulation and in hardware of the full system. It will also discuss problems that were encountered and how they were solved or why they could not be resolved. Chapter 6 relates the unsolved problems to points for future work. Chapter 7 is the conclusion.

Chapter 2

BACKGROUND

2.1 Nonlinear Interaction of Ultrasonic Waves in Air

The pioneering theoretical work behind the parametric acoustic array was done by Westervelt in 1963, who studied the scattering of sound by sound [3]. He observed that two sinusoidal ultrasonic waves of frequencies f_1 and f_2 emitted from a source would interact in the air to produce nonlinear spectral components, including the difference frequency $|f_1 – f_2|$. This difference frequency is generated within the narrow beams of the primary (ultrasonic) waves, similar to the end fire array of an antenna, giving it a relatively narrow directivity. The approximate half power angle of the generated secondary wave is

$$\theta_h \approx \sqrt{2\alpha_T/k} \tag{1}$$

where k is wavenumber of the difference frequency and α_T is the total sound absorption coefficient. Based on this equation, the directivity of the secondary wave is independent of aperture size; narrowing can be achieved by increasing the difference frequency or decreasing the primary frequencies (to lower α_T).

Westervelt's work was expanded on by Berktay [4], whose analysis was not limited to single tone primary waves. His research was on pulses produced by the interaction of a modulated carrier wave in a nonlinear medium. Given a modulated primary wave of the form $\mathrm{p_1 = p_0 E(t)\sin(\omega_c t)}$, where p_0 is the pressure source amplitude, and E(t) is the modulation envelope function, Berktay developed an expression for the demodulated secondary wave sound pressure along the axis of propagation,

$$p_2(t) \approx \frac{\beta p_0^2 a^2}{16\rho_0 c_0^4 z\alpha_0}\frac{d^2}{dt^2}E^2(t) \tag{2}$$

where β is the nonlinearity coefficient, a is the aperture radius, ρ_0 is the medium density, c_0 is the speed of sound, z is the distance along the axis of propagation, and α_0 is the absorption coefficient of the primary wave. The key takeaways from this equation are the following:

- The secondary wave sound pressure level is proportional to the square of the ultrasound level, which is beneficial for efficiency in output power; doubling the primary wave amplitude would quadruple the SPL of the demodulated wave
- The secondary wave is proportional to the square of the modulation envelope which means the demodulation would incur severe harmonic distortion
- The double derivative effect on the envelope means that lower frequency secondary signals require more intense ultrasound compared to higher frequency waves. There is approximately a +40dB/decade high pass characteristic on the down converted signal.

It should be noted that this equation is only useful in the far-field, also known as the Rayleigh distance [5], where ultrasonic wavefronts begin to rapidly attenuate and nonlinear interaction no longer occurs in the medium. Additionally, this model is limited to cases where the primary source pressure is relatively low so that the parametric array is determined by small-signal absorptions of the primary waves. However, many of the signal processing schemes and system design choices in parametric arrays are based off Berktay's equation and tend to operate within the aforementioned constraints. The next section discusses the evolution in modulation techniques and design of PAAs.

2.2 History of Parametric Loudspeaker Design

The first practical design of parametric speakers was done by Yoneyama [6], who used traditional amplitude modulation or double sideband amplitude modulation (DSB-AM) to condition the carrier. As per communications theory this system has an envelope function $\mathrm{E(t)} = 1 + \mathrm{mg(t)}$, where m is the modulation depth and g(t) is the input audio signal. Figure 2 illustrates the block diagram of the system.

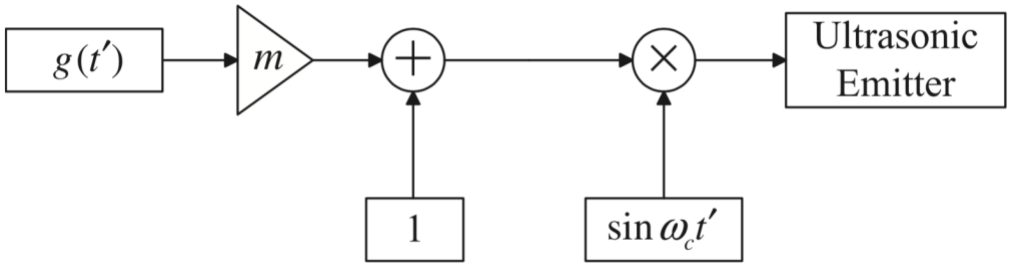

Figure 2: DSB-AM Block Diagram [2012_Gan, Yang, and Kamakura]

However, this system experienced large second harmonic distortion proportional to m_2, which is consistent with the square relationship between the secondary wave and the modulation envelope in Berktay's equation. Simply reducing m was not a viable solution either, since the output signal level is proportional to the modulation depth and lowering m would compromise the signal strength. This tradeoff between output level and harmonic distortion makes DSBAM impractical for high quality audio output.

Since then, there have been several AM based preprocessing schemes that aimed to reduce total harmonic distortion (THD), based on Berktay's solution of nonlinear demodulation. One such scheme is square root amplitude modulation (SRAM), which takes the square root of the envelope function as a means of counteracting the squaring effect on the envelope during demodulation [7]. This method is effective in reducing the overall distortion, bringing the THD to around 5%. It was successfully implemented in the Audio Spotlight, a commercial product developed by Joseph Pompei. However, it does introduce other complications.

When a signal is square-rooted, it generates an infinite series of harmonics making the bandwidth of the signal relatively large. As a result, the transducer driven by the system needs to have a sufficiently wide bandwidth to capture the harmonics of the emitted wave. Pompei and his team accomplished this by custom building a transducer with a 21kHz passband, sufficient to cover all audio frequencies. The frequency range of the transducer is shown in Figure 3. In comparison, a typical “off-the-counter” ultrasonic transmitter has a bandwidth of 1kHz.

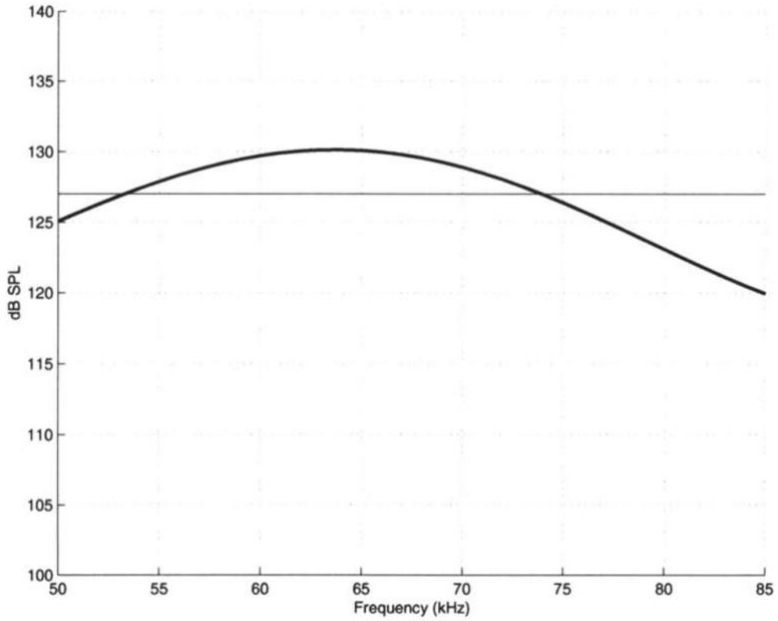

Figure 3: Frequency Response of Custom-Built Wideband Transducer. -3dB points at 53kHz and 74kHz [Pompei_2002]

The message signal is also preprocessed with a double integration to counteract the double derivative effect from Berktay’s equation.

Later, Kamakura developed a solution to reduce distortion as well as power consumption through single sideband amplitude modulation (SSB-AM) [8]. Here, the message signal is phase shifted 90_o via a Hilbert transform, and the two signals modulate orthogonal carriers $\cos(w_c t)$ and $\sin(w_c t)$. The modulated signals can be either summed or subtracted to produce lower or upper sideband modulation, respectively. This method is especially useful because it has a similar modulation envelope to that of DSB-AM, while having lower distortion and half the bandwidth.

Another unique method that has been shown to work is a Pulse Width Modulation (PWM) system, which has been used on smaller scale homebrew projects [9]. Here, the audio signal modulates the duty cycle of pulses in a high frequency pulse train signal; the higher the instantaneous amplitude of the audio signal, the greater the duty cycle. In other words, a low frequency signal is sampled and encoded in a pulse train with continually changing pulse widths. This is depicted in Figure 4.

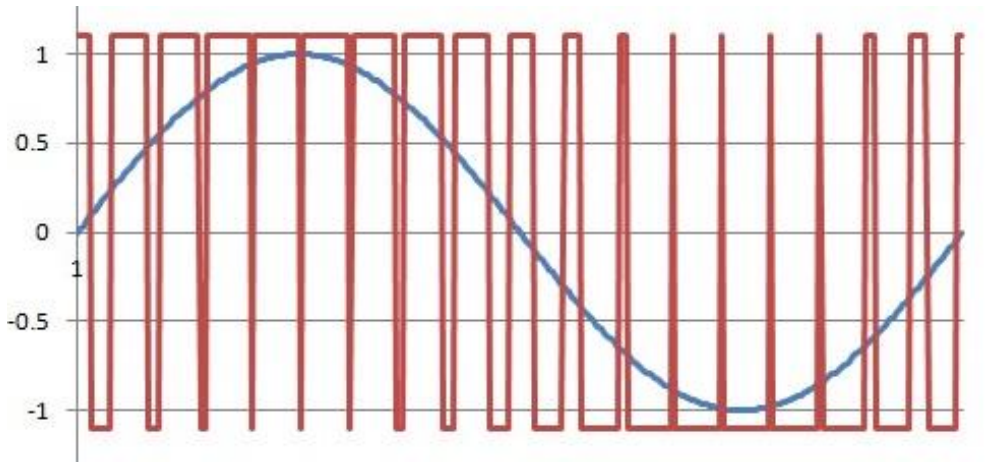

Figure 4: Arbitrary PWM Waveform: Low Frequency Blue Signal Modulating High Frequency Red Pulse Train

The utility of PWM is that it generates a spectrum that is similar to DSB-AM but with added harmonic content. This harmonic content needs to be filtered out with a bandpass filter, so out of both necessity and convenience, these systems can use inexpensive narrowband transducers. PWM is explained in further detail in Section 2.6.

2.3 Polyphase Filters

Polyphase networks or polyphase filters are multiple input multiple output (MIMO) filters that discriminate based on frequency and the sequence of inputs [10]. The sequence of inputs is defined by the relative phase between the input signals. As a simple example, a four-input sequence is shown in Figure 5. The first signal is cos(ωt), and the sequence shifts the phase by -90₀ from input to input. The full sequence is $\cos(\omega t) \rightarrow \sin(\omega t) \rightarrow -\cos(\omega t) \rightarrow -\sin(\omega t)$, and this corresponds to a clockwise rotating vector as shown by the phasor representations of the signals. This sequence is referred to as a “negative” sequence because the phase rotation is negative. The sequence is also considered a balanced set because their corresponding vectors have a net zero sum.

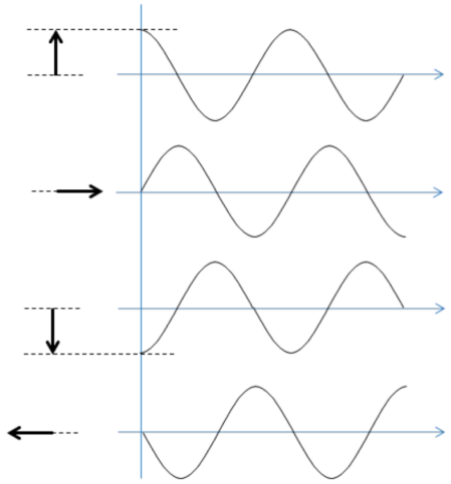

Figure 5: Vector Representation and Time Domain Waveforms of Negative Input Sequence [Prodanov_2018]

In general, the four input signals will not be a balanced quadrature set but rather an unbalanced set made up of a summation of positive or counter clockwise rotating vectors and negative or clockwise rotating vectors. This is illustrated in Figure 6. As the signals propagate through the filter, the filter will discriminate against a certain rotational direction, corresponding to the relative phase between the inputs, and the outputs will be either only a positive balanced sequence or only a negative balanced sequence. In other words, the outputs will be of equal magnitude but 90_0 out of phase with each other, and their order will be either in a positive rotation or a negative rotation. In Figure 7, an example polyphase network filters out the positive sequence and keeps the negative sequence.

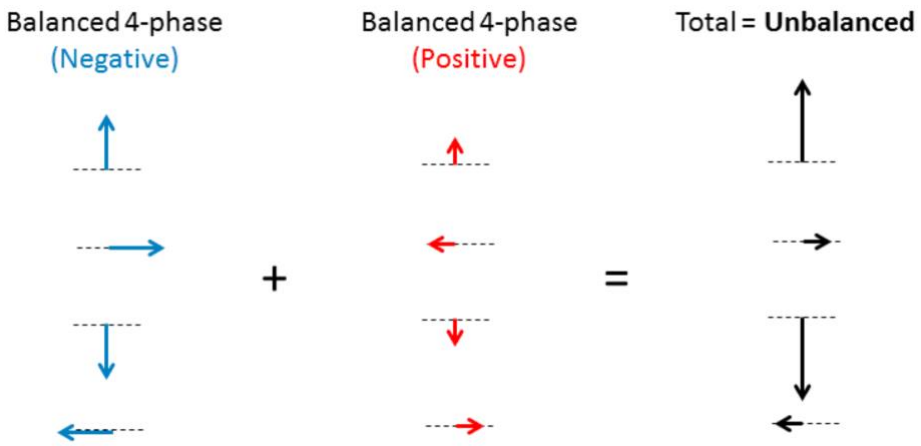

Figure 6: Unbalanced Set of Signals as Summation of Balanced Positive and Negative Sequences [Prodanov_2018]

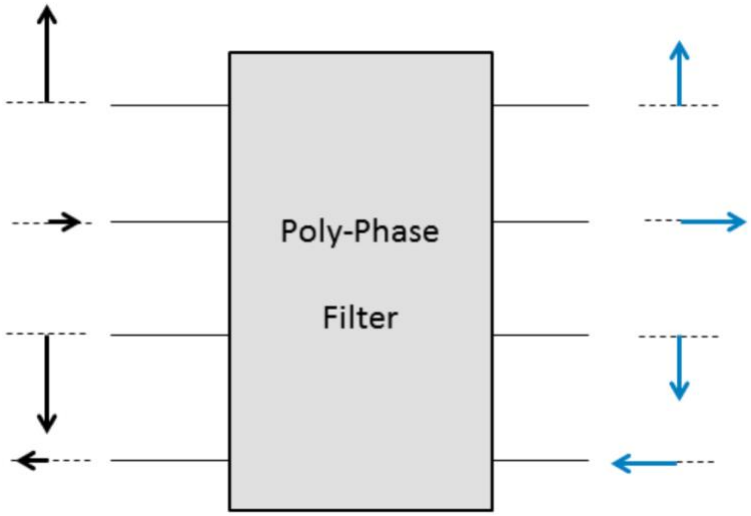

Figure 7: Polyphase Filter Extracting Negative Quadrature Sequence from Unbalanced Input Set [Prodanov_2018]

One popular analog topology is the RC Gingell Network, which is explained in [11].

2.4 Hilbert Transform, SSB-AM, and Envelope Signals

The Hilbert Transform is a linear operator used in signal processing applications, including the generation of SSB-AM signals. The time domain analysis can be quite complex, so it is best examined in the frequency domain. The Hilbert Transform phase shifts all positive frequencies of a signal by -90$_o$ and all negative frequencies by +90$_o$ [12]. The operator is defined as follows: Given a signal x(t) with a Fourier Transform X(f), the Hilbert transform of that spectrum is

$$H\{X(f)\} = \hat{X}(f) = -jsgn(f)X(f) \tag{3}$$

$$sgn(f) = \begin{cases} 1, & f > 0 \\ -1, & f < 0 \end{cases} \tag{4}$$

As a simple example, consider the function cos(ωt). Since this signal has a single frequency component, the Hilbert Transform can be easily computed as cos(ωt – 90$_o$) = sin(ωt). In other words, the Hilbert Transform of cosine is the sine function.

For any real valued arbitrary signal x(t), there are positive and negative frequency components in the spectrum. The analytic signal x$_a$(t) is a complex signal which is defined as the following:

$$x_a(t) = x(t) + j\hat{x}(t) \tag{5}$$

Where $\hat{x}(t)$ is the inverse Fourier transform of $\hat{X}(f)$ or the Hilbert transform of x(t). The beauty of the analytic signal is that its spectrum contains only the positive spectral components of x(t).

$$\frac{1}{2}X_a(f) = \begin{cases} X(f), & f > 0 \\ 0, & f < 0 \end{cases} \quad (6)$$

This property is what makes single sideband modulation possible. A frequency shifted version of the analytic signal $X_a(f-f_c)$ contains only the upper side of the spectrum of X(f), referenced at the carrier frequency f_c. Also since this signal contains only positive frequencies, it is the analytic single sideband modulated signal. The real single sideband modulated signal is obtained by taking the real part of the shifted analytic signal and discarding the imaginary component.

$$X_a(f - f_c) \overset{I.F.T}{\Longrightarrow} x_a(t)e^{j2\pi f_c t}$$

$$x_{USB}(t) + j\hat{x}_{USB}(t) = x_a(t)e^{j2\pi f_c t}$$

$$x_{USB}(t) = Re\{x_a(t)e^{j2\pi f_c t}\}$$

$$x_{USB}(t) = Re\{\,[x(t) + j\hat{x}(t)] \times [\cos(2\pi f_c t) + jsin(2\pi f_c t)]$$

$$x_{USB}(t) = x(t)cos(2\pi f_c t) - \hat{x}(t)\sin(2\,\pi f_c t) \quad (7)$$

Equation 7 computes the time domain representation of the upper sideband modulation with a suppressed carrier [13]. Continuing with the example of a cosine input, the upper sideband signal is computed as shown in the block diagram in Figure 8, where x(t) = Acos(ωmt) and its Hilbert transform is Asin(ωmt).

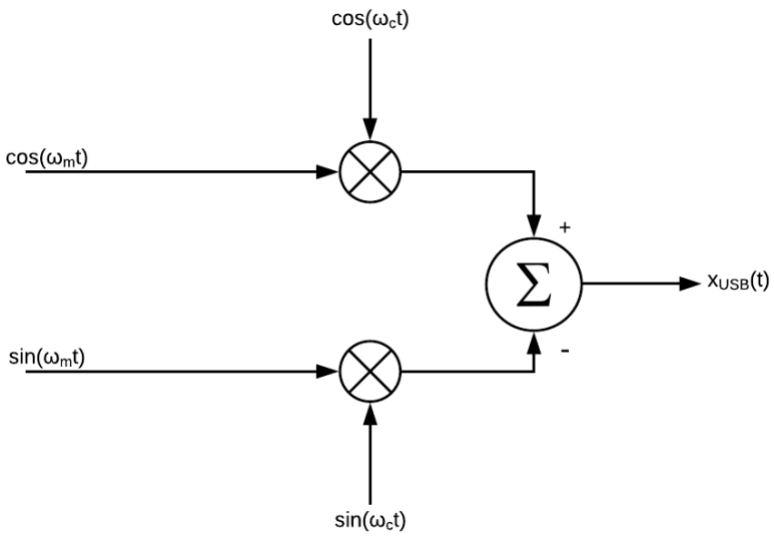

Figure 8: Upper SSB-AM Block Diagram with Sinusoidal Input

$$x_{USB}(t) = Acos(\omega_m t)cos(\omega_c t) - Asin(\omega_m t)\sin(\omega_c t) \quad (8a)$$

Using the trigonometric identity cos(a+b) = cos(a)cos(b) – sin(a)sin(b), we simplify the expression above.

$$x_{USB}(t) = Acos((\omega_c + \omega_m)t) \tag{8b}$$

As expected, the computation produces a single tone at the sum frequency of the carrier and message signal. By extension, it can be deduced that any arbitrary signal with a finite or infinite series of Fourier components can go through the same process to produce a frequency shifted version of its upper sideband. Once again, this modulated signal is a suppressed carrier signal, meaning its spectrum does not contain the carrier frequency. In some applications this is acceptable, but in parametric arrays the carrier is needed for nonlinear demodulation to be possible. The general form of the upper SSB-AM block diagram is shown in Figure 9, with the carrier added at the end.

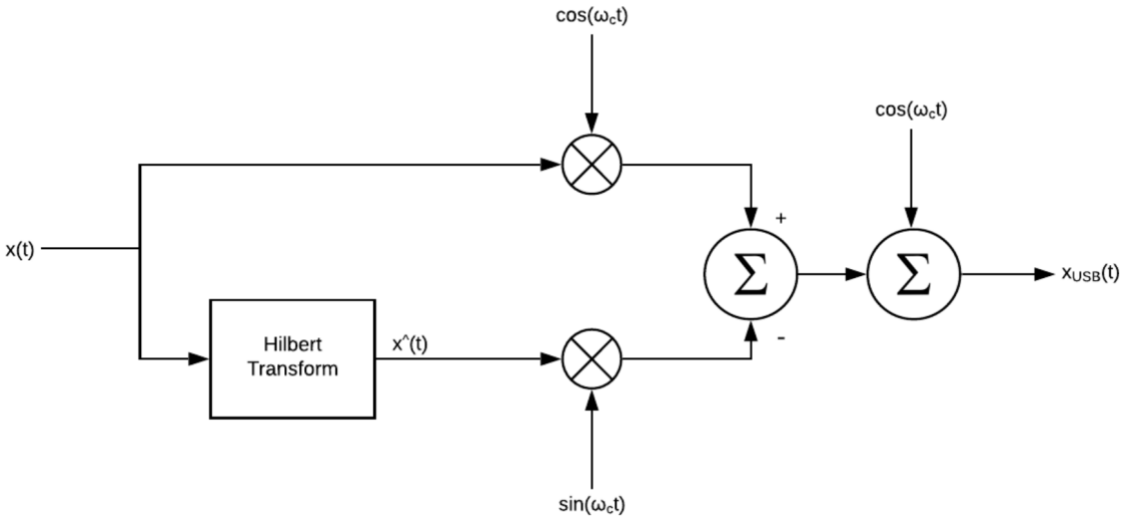

Figure 9: General Form of Upper SSB-AM with Carrier Signal

The envelope function E(t) of a multi-tonal signal such as the SSB-AM signal with the carrier is computed with the analytic signal as outlined in [14]. We are interested in this because in nonlinear demodulation the output is proportional to the envelope squared of the primary signal. Given a multi-tonal input x(t), we take the Hilbert transform $\hat{x}(t)$ which is the imaginary component of the envelope. The magnitude of the envelope function is defined as the following

$$|E(t)| = \sqrt{x^2(t) + \hat{x}^2(t)} \tag{9a}$$

$$E^2(t) = x^2(t) + \hat{x}^2(t) \tag{9b}$$

2.5 Monostable Multi-vibrators

One way of creating PWM signals is with 555 timers in monostable mode [15]. The pulse is triggered with an active low trigger signal, and the timing is determined by a charging capacitor on the timer threshold pin. In the case of Figure 10, the capacitor charges by a constant voltage source, at a rate determined by the RC constant of the components connected to the timer. Once the threshold is crossed, the output voltage goes low and the pulse is created.

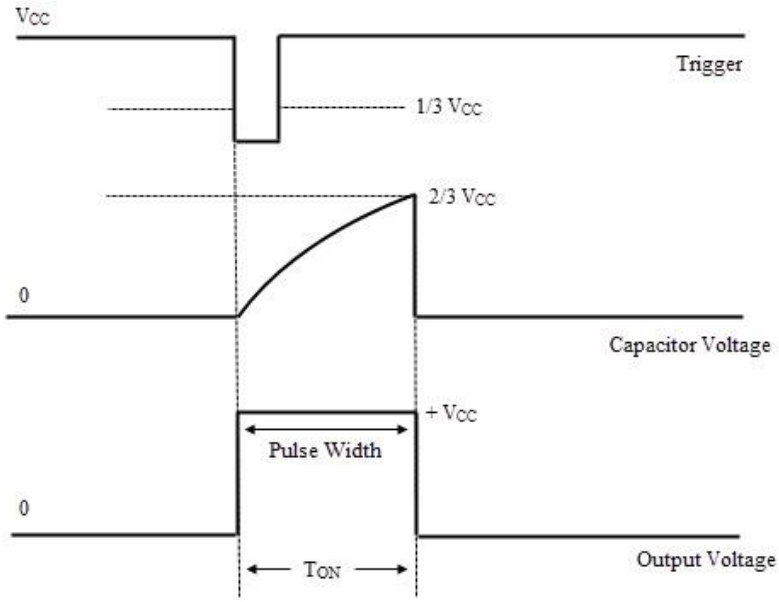

Figure 10: 555 Timer Based Monostable Multi-vibrator Timing Diagram

2.6 Pulse Width Modulation

At its core, a pulsing signal is a square wave, which means its Fourier Series contains the fundamental frequency and an infinite series of odd harmonics [16]. When an analog sinusoidal signal modulates the pulses, we see sidebands appear near the fundamental frequency, similar to DSB-AM. However, we also see replicas of the modulated carrier at each harmonic. The formula for sideband locations is defined as:

$$f_{harm} = nf_c \pm f_m; n = 1,2,3, \ldots \quad (10)$$

where f_c is the fundamental carrier frequency and f_m is the modulating signal frequency. However, this is not the only set of harmonics that appear in the spectrum of a PWM wave. For each replica of the modulated carrier, there is a decaying set of harmonics of the modulating frequency that decay as they get further from the carrier harmonics. This is illustrated in Figure 11 where we see a 40kHz carrier square wave modulated by a 5kHz sine wave.

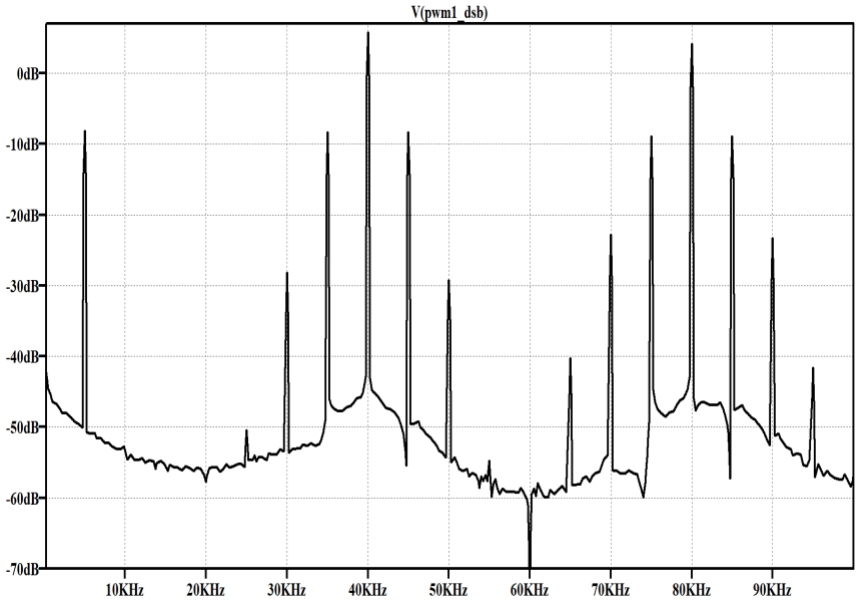

Figure 11: PWM Spectrum. Fundamental Frequency f_c = 40kHz, Modulating Frequency f_m = 5kHz

The modulated carrier spectrum appears at 40kHz and is repeated at 80kHz, with decaying tones that are spaced 5kHz from each other. This is a typical PWM frequency response, and the reason it appears this way is because PWM is a nonlinear process itself. The graph in Figure 12 shows the relative amplitude of the first few harmonics of the carrier frequency as a function of the pulse duty cycle [17].

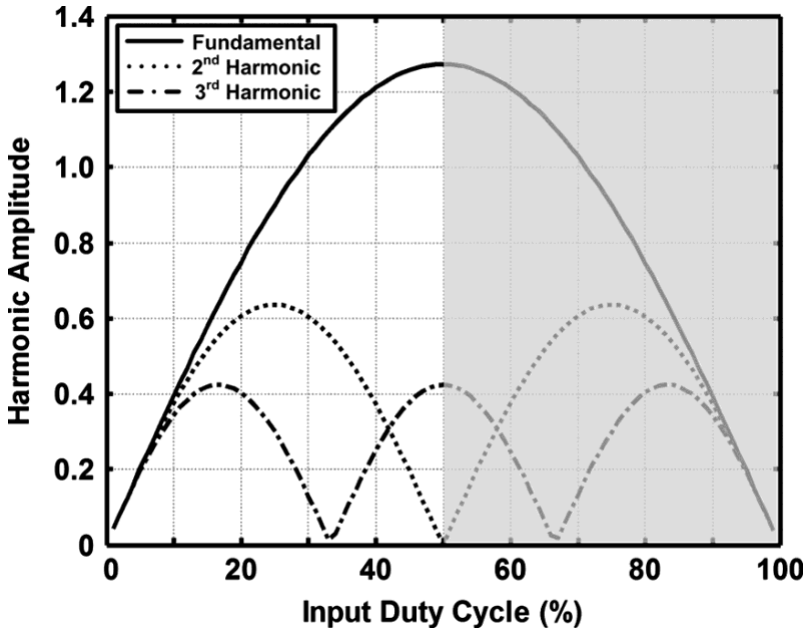

Figure 12: Amplitudes of PWM Harmonics vs. Duty Cycle [2009_Walling]

There is a sinusoidal relationship between the relative amplitudes of the carrier harmonics and the instantaneous duty cycle of a PWM wave. In Figure 12 the solid line plot represents the 1st harmonic, or the fundamental frequency of the signal. Its relative amplitude is governed by the equation

$$Fun = \frac{A}{\pi}\sin(D\pi) \tag{10}$$

where A is the pulse amplitude and D is the duty cycle of the wave. When the function above is multiplied by the fundamental frequency signal, it creates distortion terms that appear at harmonics of the modulating frequency, referenced from the fundamental frequency.

2.7 Series Resonance

In a series RLC circuit, there is an operating point known as series resonance where the reactance of the inductor and the capacitor equal each other and their impedances cancel each other out, making the circuit purely resistive [18]. The frequency at which this occurs is the resonant frequency of the circuit. The circuit is shown in the Figure 13 below. The total impedance in series resonance is evaluated.

$$Z_T = R + jX_L - jX_C \tag{11a}$$

$$X_L = X_C$$

$$Z_T = R \tag{11b}$$

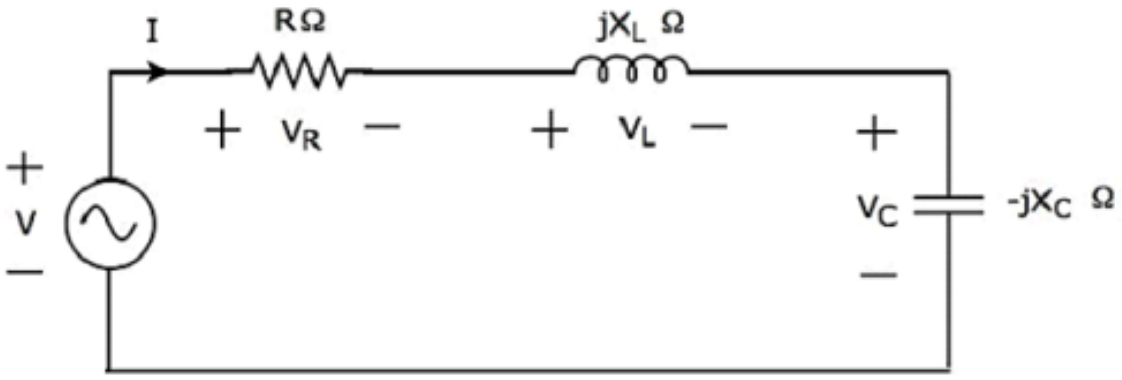

Figure 13: Series RLC Circuit

Since the system is purely resistive at the resonant frequency, the voltage across the resistor is maximized, and this is where the resonant peak occurs. Generally, voltage driven narrowband transducers have a similar frequency response and can therefore be modelled as a series RLC circuit in simulation. Section 3.2 clarifies this statement

Chapter 3

PRELIMINARY WORK

3.1 Philosophy Behind SSB-PWM

With a deeper understanding of both SSB-AM and PWM, it seems logical to explain how an SSB spectrum can be generated purely from PWM signals and why it is appropriate to take this approach for signal processing in parametric acoustic arrays. The idea was initially proposed for radio frequency applications by Raab [19]. While a “normal” PWM system is directly concerned with the baseband signal, an RF PWM system is interested in the frequency content around the harmonics of the PWM signal. Thus, instead of using a low pass filter to extract the DC signal, an RF PWM system uses a tuned bandpass filter to extract a particular harmonic and the energy surrounding it.

Raab’s paper continues by asserting that two RF PWM systems can be combined to produce an SSB-AM waveform. When a phase shifted carrier and audio input $x_i(t)$ are applied to one RF PWM, and a carrier and phase shifted audio signal $x_q(t)$ are applied to another, the sum of the signals will produce an SSB spectrum. The two signals can be either interlaced or overlapped when they are summed. In Figure 14 both of these methods are shown with bipolar PWM signals.

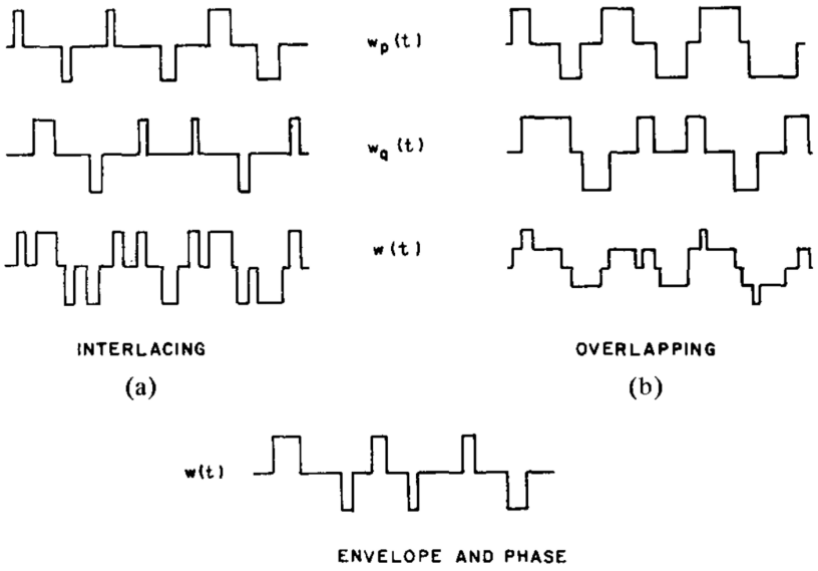

Figure 14: Techniques for Producing SSB Spectrum with Bipolar PWM Signals [1973_Raab]

This PWM based SSB generation can be carried over to an ultrasonic frequency with unipolar pulsing signals that are interlaced to maintain a two-level output. The first PWM signal is modulated by a -90_o phase shifted version of an audio signal and the second PWM signal is modulated by the audio signal. The second PWM signal is delayed by 25% of a full cycle, which shifts its fundamental frequency phase by -90_o. The duty cycles of both signals are kept below 25% to prevent overlapping. When the two PWM signals are summed, the passband region of interest surrounds the fundamental harmonic, because this is where the SSB-AM occurs. The time domain representation of this signal is shown in Figure 15, and the block diagram is shown in Figure 16.

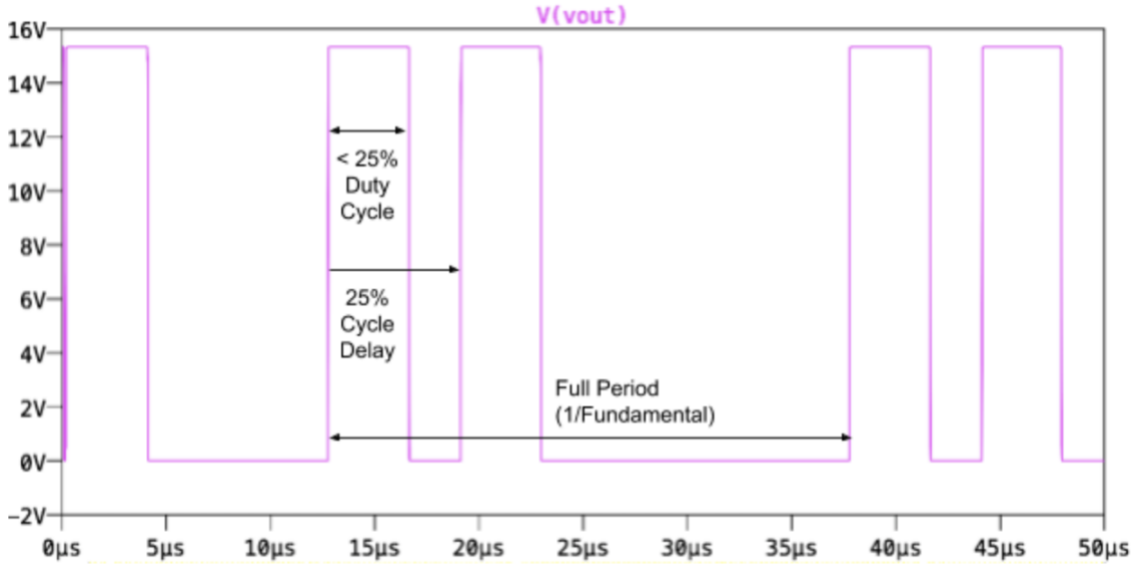

Figure 15: Time Domain Representation of SSB-PWM Signal

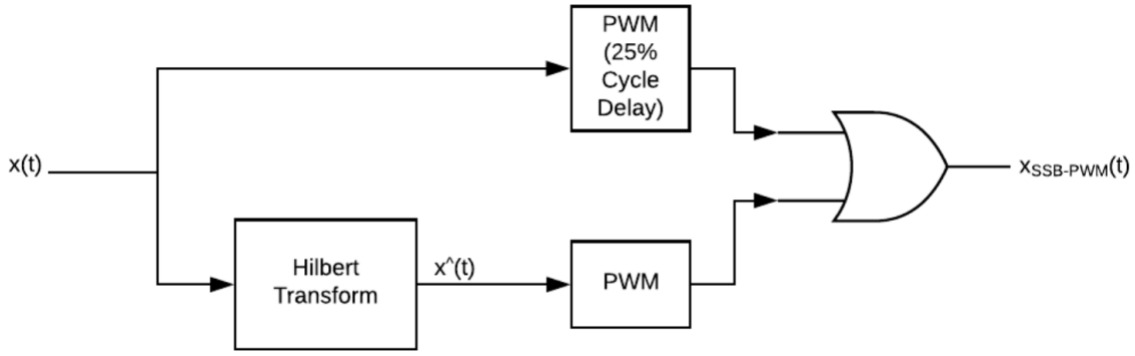

Figure 16: SSB-PWM System Block Diagram

3.2 Ultrasonic Transducer Impedance Characterization

In order to drive the transducers at the optimal frequency and amplitude, they need to first be characterized for impedance and frequency response. The transducer used was the MSO-P1040H07T [20], a 10 mm ultrasonic transmitter with a center frequency of 40kHz and a large drive capability of up to $40V_{rms}$. The test circuit in Figure 17 is used to measure the voltage across the transducer V_T, which is then used to calculate its impedance over a range of frequencies.

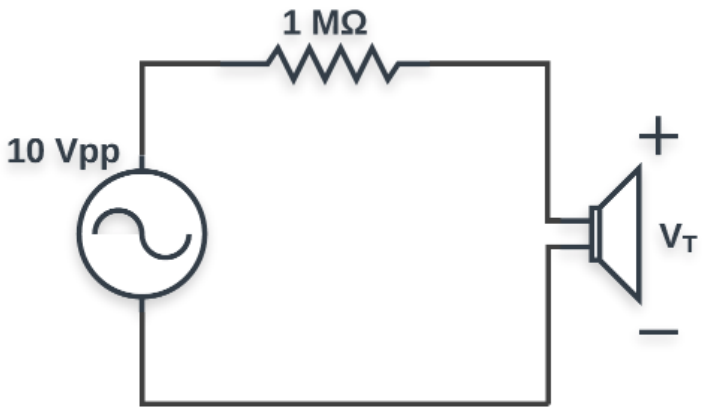

Figure 17: Transducer Impedance Measurement Circuit

Using this setup, the circuit creates the following voltage divider relationship:

$$V_T = V_{in} * \frac{Z_T}{Z_T + R} \tag{12a}$$

Here, V_{in} is the 10V peak to peak input voltage, Z_T is the transmitter impedance, and R is the 1MΩ resistor in series with the transducer. Given a sufficiently large R value, the equation can be simplified and solved for the transmitter impedance:

$$V_T \approx V_{in} * \frac{Z_T}{R}$$
$$Z_T \approx \frac{V_T R}{V_{in}} \tag{12b}$$

The input voltage is swept from 35 kHz to 45kHz and Z_T is calculated. The blue plot points in Figure 18 represent the calculated impedance values.

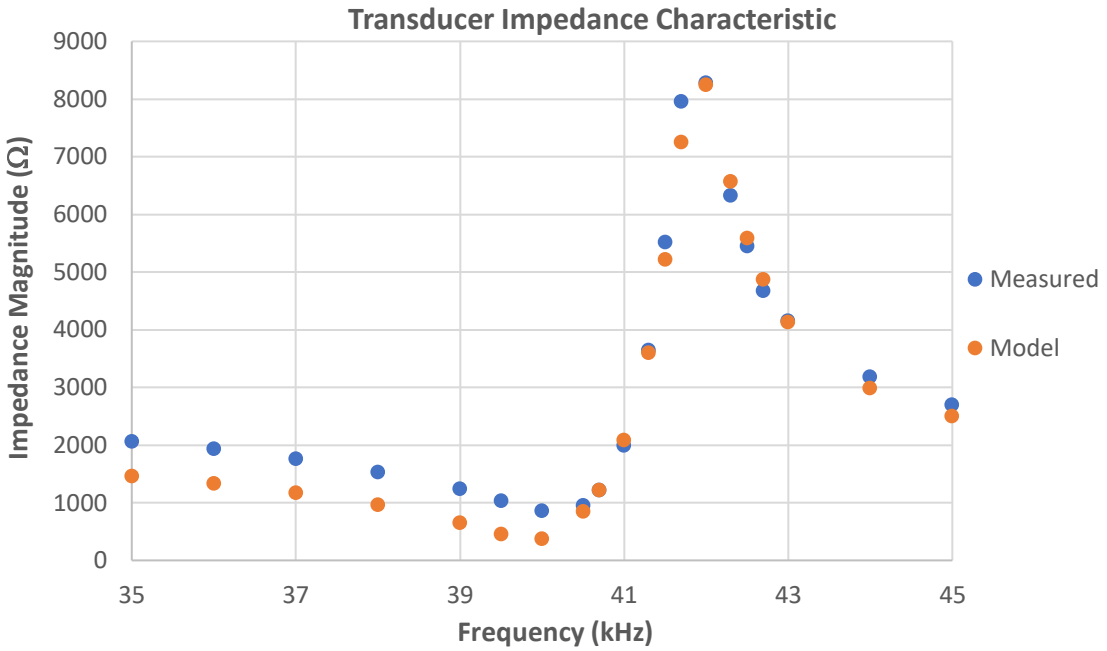

Figure 18: MSO-P1040H07T Ultrasonic Transmitter Impedance Measurement and Equivalent Impedance Model Plots

The trough and the peak in the impedance response are indicative of both series and parallel resonance in the transducer. Outside these regions, the impedance is capacitive in nature. Using this information, an equivalent impedance model is generated.

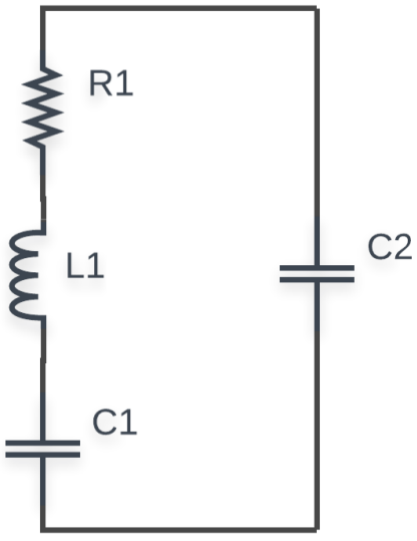

Figure 19: MSO-P1040H07T Transducer Equivalent Impedance Model

The total impedance of the circuit in Figure 19 is evaluated to be

$$Z_{tot}(s) = \frac{s^2 L_1 C_1 + s C_1 R_1 + 1}{s^3 L_1 C_1 C_2 + s^2 C_1 C_2 R_1 + s C_2 + s C_1} \tag{13a}$$

From this, the magnitude of the impedance can be solved:

$$|Z_{tot}|(\omega) = \frac{\sqrt{(1 - \omega^2 L_1 C_1)^2 + \omega^2 {C_1}^2 {R_1}^2}}{\sqrt{\omega^4 {C_1}^2 {C_2}^2 {R_1}^2 + \omega^2 (C_1 + C_2 - \omega^2 L_1 C_1 C_2)^2}} \tag{13b}$$

Using Equation 13b, the four component values R1, L1, C1, and C2 can be solved for in software. For this computation, the solver in Microsoft Excel was used to minimize the average error between the measured impedances and the ones computed by Equation 13b at 20 different frequency values. The resulting component values are shown in Table 1, which produces the orange plot points in Figure 18 on the previous page.

Table 1: Transducer Equivalent Impedance Component Values

R1	**L1**	**C1**	**C2**
370 Ω	74.5 mH	213 pF	2.2nF

From here the frequency response of the transducers can be evaluated. Since the resistor R1 is the only dissipative element in the circuit in Figure 19, it represents the conversion of electrical energy to acoustic energy. The transfer function is the ratio between the resistor voltage and the input voltage. Also, the capacitor C2 does not affect the transfer function because the circuit is assumed voltage driven, and C2 is in parallel with the rest of the circuit. Thus, it can be ignored. The transfer function is derived by first writing the voltage across R1.

$$V_{R_1}(s) = \frac{R_1}{R_1 + sL_1 + \frac{1}{sC_1}} V_{in} \tag{14}$$

Multiplying the top and bottom by sC_1 and converting from the Laplace domain to the frequency domain, we get the frequency response of the system and subsequently the magnitude response.

$$H(\omega) = \frac{j\omega C_1 R_1}{-\omega^2 L_1 C_1 + j\omega C_1 R_1 + 1} \tag{15a}$$

$$|H(\omega)| = \frac{\omega C_1 R_1}{\sqrt{(1 - \omega^2 L_1 C_1)^2 + (\omega C_1 R_1)^2}} \tag{15b}$$

This is the frequency response of a bandpass filter. The magnitude response can be rewritten in a form which allows us to evaluate the center frequency ω_o and the Q factor of the filter.

$$|H_{BP}(\omega)| = \frac{1}{\sqrt{1 + Q^2\left(\frac{\omega_o}{\omega} - \frac{\omega}{\omega_o}\right)^2}} \tag{16}$$

In equation 16, $Q \equiv \frac{\sqrt{L/C}}{R}$ and $\omega_o = \frac{1}{\sqrt{LC}}$. Using the component values from the equivalent impedance circuit, we have Q = 50.5 and $\omega_o = 2.510 * 10^5$ rad/sec. f_o can be easily calculated by dividing ω_o by 2π to obtain $f_o = 39.95$ kHz. This is consistent with the 40kHz rated frequency of the MSO-P1040H07T. The plot of the frequency response is shown in Figure 20.

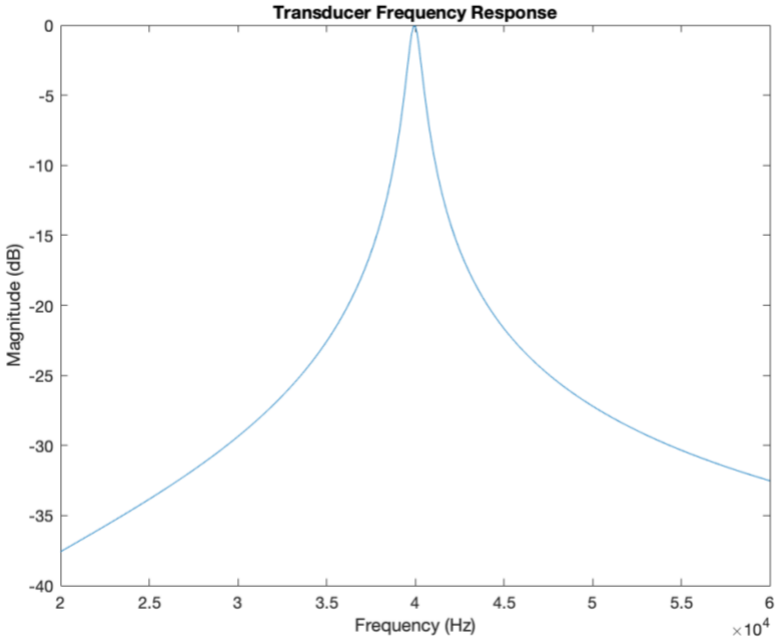

Figure 20: MSO-P1040H07T Transducer Frequency Response

Recall in section 2.2 that a few of the previous designs for parametric acoustic arrays used a double integrator to preprocess the audio-band signal, which then drove a transducer with a wideband response. For this system, however, the narrowband response of the transducer can provide a free integration without additional components. Imagine the spectrum around the first harmonic of the PWM driving signal to be centered at the resonant frequency of the transducer (40kHz). The two sidelobes of the frequency response behave like first order lowpass filters on the upper and lower sidebands of the modulated ultrasonic signal. This is proven by comparing each sidelobe to a first order integrator with a specified cutoff frequency and a -20dB/decade roll-off trend.

The second order bandpass magnitude response in equation 16 is split into a two-piece first order approximation as follows:

$$|H_{LSB}(f)| = \frac{1}{\sqrt{1 + \left(\frac{f - f_o}{f^-}\right)^2}}, \qquad f \le f_o \tag{17a}$$

$$|H_{USB}(f)| = \frac{1}{\sqrt{1 + \left(\frac{f - f_o}{f^+}\right)^2}}, \qquad f \geq f_o \tag{17b}$$

The first equation represents the lower half of the bandpass filter response (below 39.95kHz) and the second equation represents the upper half (above 39.95kHz). F^- and f^+ are the -3dB cutoff frequencies of the lower sideband and the upper sideband, respectively, measured as the distance away from the center frequency. By plotting each half of the second order filter response and comparing them to the first order responses, f^- and f^+ can be tuned to minimize the error between the two plots. The optimal values are $f^- = 370$Hz and $f^+ = 460$Hz, and the comparisons can be seen in Figure 21.

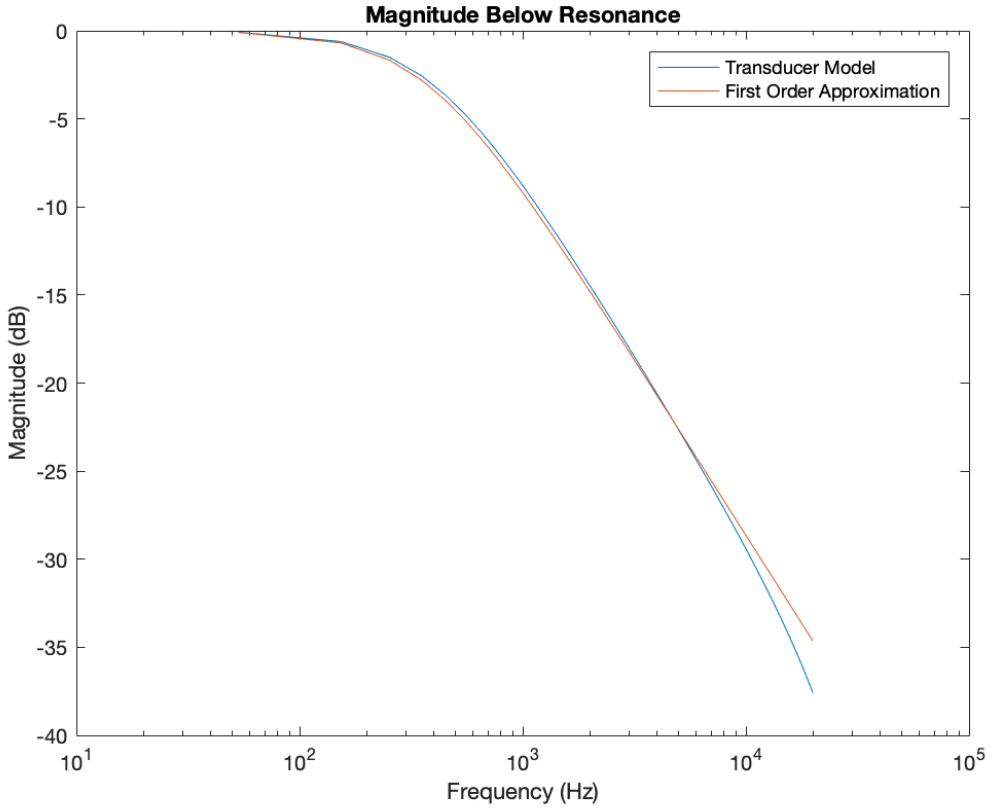

(a)

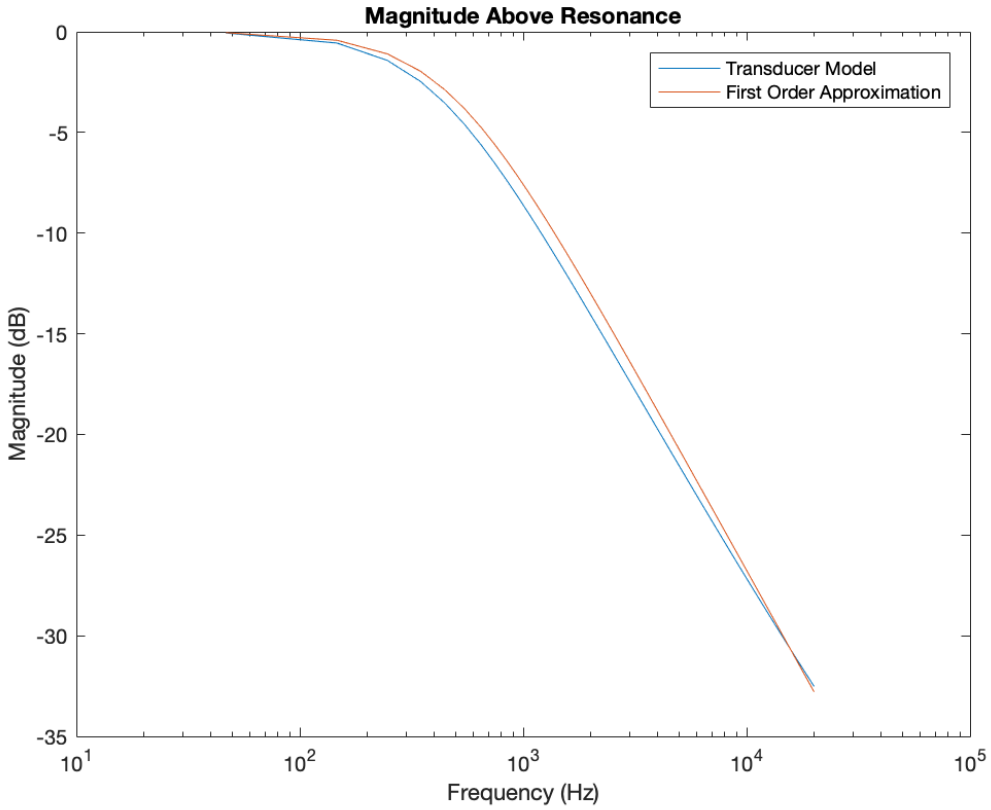

(b)

Figure 21: Comparing the Sideband Magnitude Responses of MSO-P1040H07T with a First Order Integrator. (a) Lower Sideband (f_- = 370Hz). (b) Upper Sideband (f_+ = 460Hz).

These plots justify the use of narrowband transducers in parametric acoustic arrays. They have the same low-pass effect of an integrator that would otherwise be used in the back-end of the design, and they are far cheaper than building a transducer with a broadband response.

3.3 Design Simulation

Prior to purchasing any hardware components, a simulation of the full SSB-PWM circuit was built in LTSpice as shown in Figure 22. The simulation takes in an input audio frequency signal and outputs a 40kHz fundamental SSB-PWM signal. The details of this circuit and all of its subsystems will be explained in Chapter 4, but it can be seen in the output FFT of Figure 23 that the system produces an upper SSB spectrum around the 40kHz fundamental frequency. In that particular case the input is a 5kHz sine wave, and the FFT shows a large magnitude response at 45kHz, 5kHz above the fundamental. By contrast, the FFT has a suppressed magnitude 5kHz below the fundamental frequency at 35kHz, confirming the single sideband nature of the frequency response.

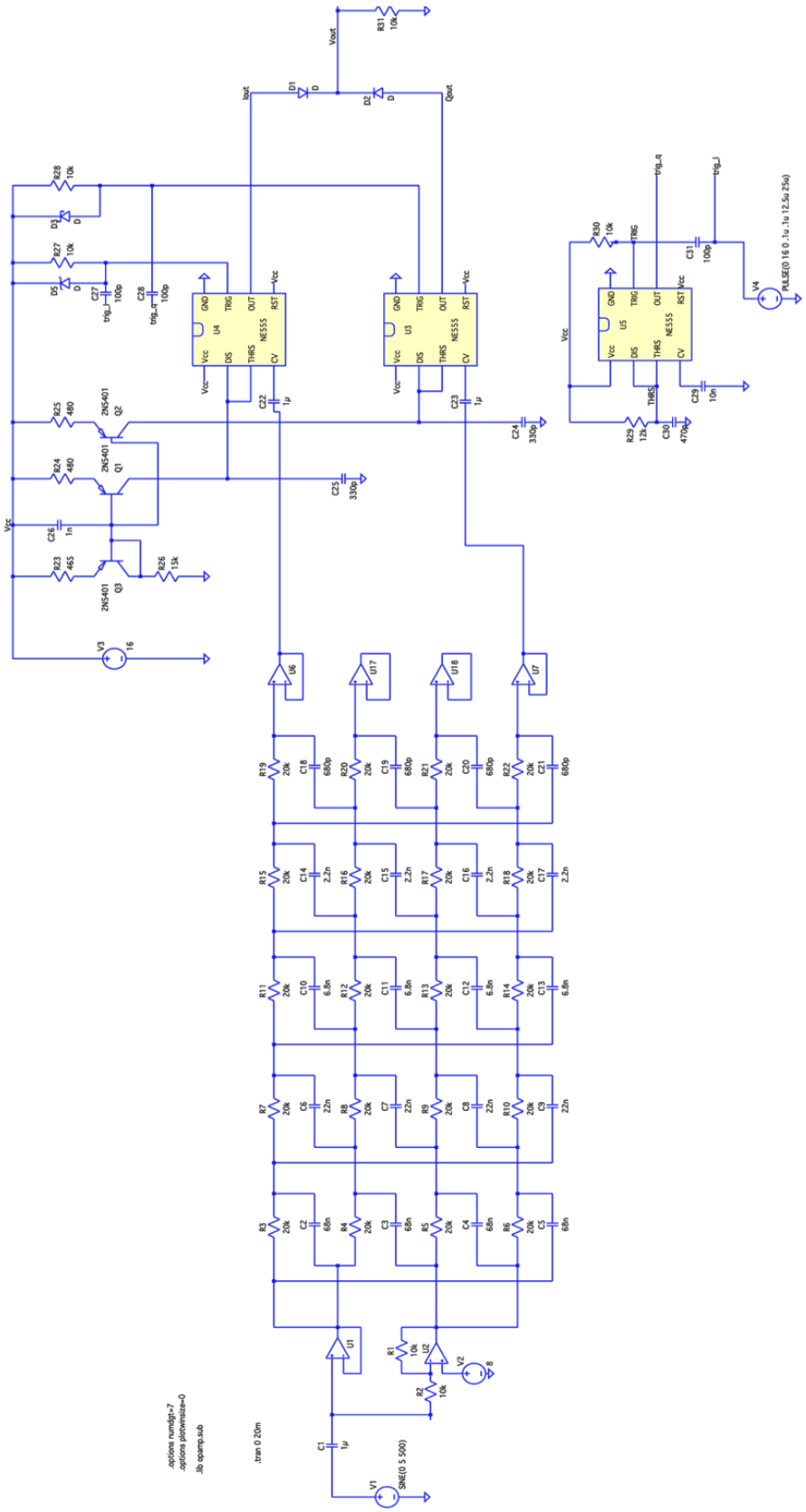

Figure 22: SSB-PWM Simulation Circuit

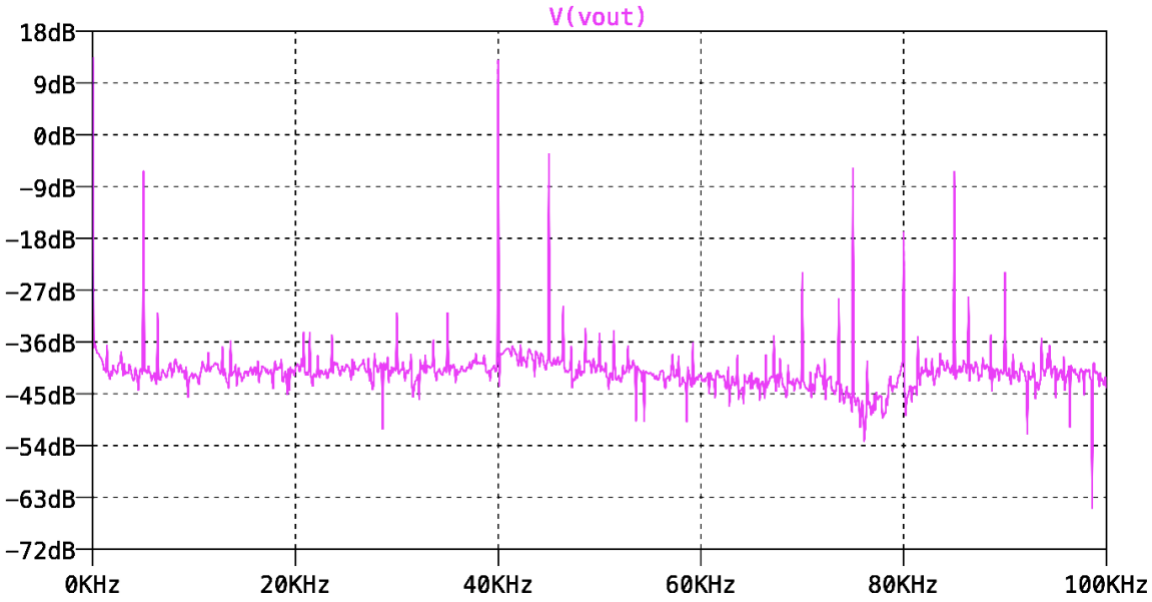

Figure 23: SSB-PWM Simulation Output Voltage FFT. Fundamental Frequency f_f = 40kHz, Modulating Frequency f_m = 5kHz

If we drive an array of narrowband transducers centered at 40kHz, the transducers will behave as a bandpass filter that selects the frequency content around the fundamental and performs a first order integration on that frequency content. This eliminates the need for a second integrator in the processor, assuming that the effects of integration on the input are the same before and after pulse width modulation.

3.4 System Specifications

The system specifications were also defined before buying components, and they are shown in Table 2. The supply voltage needs to be sufficiently large enough for the system to produce an audible demodulated signal, while being suitable for common op-amps and other integrated circuits. Typically, in the demodulation process there is a -40dB attenuation between the modulated ultrasonic signal and the audible secondary wave, so transmitters need to emit at least 120dB SPL.

Table 2: Hardware Specifications for SSB-PWM System

Specification	**Value**
Supply Voltage	+16V
Audio Input Frequency Range	20Hz – 20kHz
Pulse Width (Duty Cycle) Range	2µs - 6µs (8% - 24%)
Pulse Separation (%Cycle)	6.25µs (25%)
Transducer Center Frequency	40kHz
Output Ultrasonic Sound Pressure Level	>120dB

Based on the specifications above, the following components were purchased for the system. The remaining components were passive components (resistors, capacitors) sourced from Dr. Prodanov and the EE department.

Table 3: Bill of Materials for Purchased Components

Part Number	**Description**	**Unit Cost**	**Quantity**	**Total Cost**
LM358-N	Low-Power, Dual Operational Amplifiers	$0.84	3	$2.52
TC4427A	1.5A Dual High-Speed Power MOSFET Drivers	$1.36	2	$2.72
4808-3004-CP	8-Pin DIP IC Socket	$0.51	8	$4.08
LM555	555 Timer	$1.00	3	$3.00
P0915N-FC15BR10K	10kΩ Rotary Potentiometer	$1.44	1	$1.44
RM065-102	1kΩ Trimmer Potentiometer	$0.25	1	$0.25
MSO-P1040H07T	40kHz Piezo Ultrasonic Transmitter	$0.80	25	$20
				TOTAL: $34.01

Chapter 4

DESIGN

4.1 Overall Design

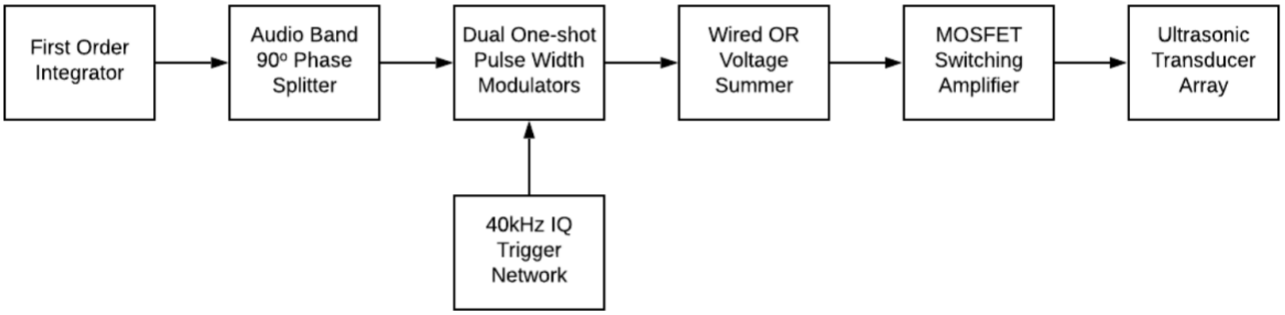

Figure 24: SSB-PWM Level 1 Block Diagram

The full system consists of several important subsystems: In the preprocessing region there is a single integrator which equalizes the input audio signal in favor of lower frequencies to make up for the high-pass effect of nonlinear demodulation. Next comes an audio band polyphase filter which generates four audio signals that are identical in magnitude but 90_o out of phase with each other. Two of these signals (with 90_o relative phase) are fed into the Control Voltage inputs of 555 timers which are used to create two pulse width modulated signals. The timers are triggered by 40kHz clock signals (I and Q) to match the resonant frequency of the ultrasonic transducers, and the audio signals modulate the output pulse widths. The I clock signal triggers its corresponding timer a quarter cycle after the Q clock, and the output duty cycles are kept below 25%. This is to ensure that the high levels of the I and Q outputs never coincide with one another, so that they can be summed without interfering with each other. Once the two outputs are summed, the result is a “SSB-PWM” signal with the harmonic content of a single sideband modulated signal near the fundamental 40kHz frequency. By sending this signal to a narrowband transducer array, the unwanted harmonics are filtered out and the passband region is filtered at -20dB/decade from the center frequency of 40kHz.

A quick comparison between SSB-PWM and a previously used modulation scheme, SRAM highlights the potential advantages of SSB-PWM. The preprocessing block diagrams are shown in Figure 25. While the SRAM system uses a double integration upfront and a wideband transducer, the SSB-PWM system uses a single integrator and narrowband transducers. The narrowband frequency response of the transducers behaves as the second integration on the SSB-PWM signal, eliminating the need for the hardware for a second integrator. The narrowband transducers are also inexpensive compared to a custom wideband ultrasonic speaker.

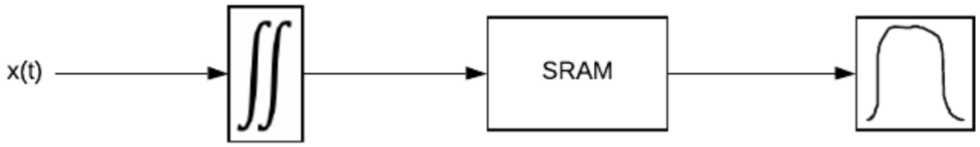

(a)

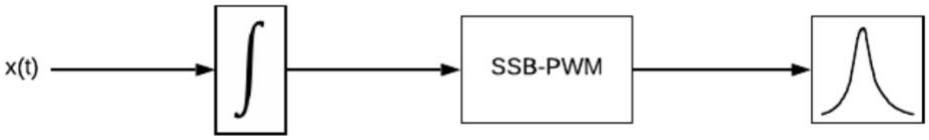

(b)

Figure 25: Block Diagrams of Preprocessing Segments of (a) SRAM Scheme and (b) SSB-PWM Scheme

4.2 Active-RC Integrator

The first subsystem in the signal chain is an op-amp integrator. It is used to equalize the audio input and counteract the double derivative effect of nonlinear demodulation. This is the first of two integrations that are applied to the input signal; the second integration occurs at the transducer array itself through the bandpass response of the transducers during conversion of electrical signals to acoustic waves.

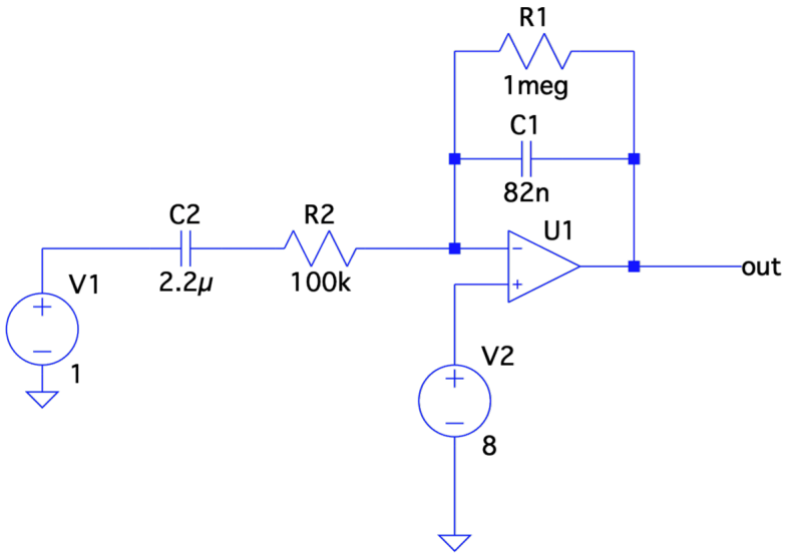

Figure 26: Active-RC Integrator Circuit Diagram

The component values in Figure 26 are chosen such that the circuit has a -3dB cutoff frequency below the audio spectrum and sufficient gain at higher frequencies. The cutoff frequency is determined by the feedback resistor and capacitor R1 and C1 from the following equation:

$$f_{-3dB} = \frac{1}{2\pi(R_1)(C_1)} = \frac{1}{2\pi(1M\Omega)(82nF)} = 1.94\ Hz \tag{18}$$

A cutoff frequency of 1.94Hz allows the integrator to be well into the -20dB/decade range when the input signal frequency reaches 20Hz, the lower end of the audio frequency range [22]. R2 is chosen such that the system has unity gain at 20Hz, which is around 100kΩ. The LTSpice simulation in Figure 27 shows the frequency response of the integrator.

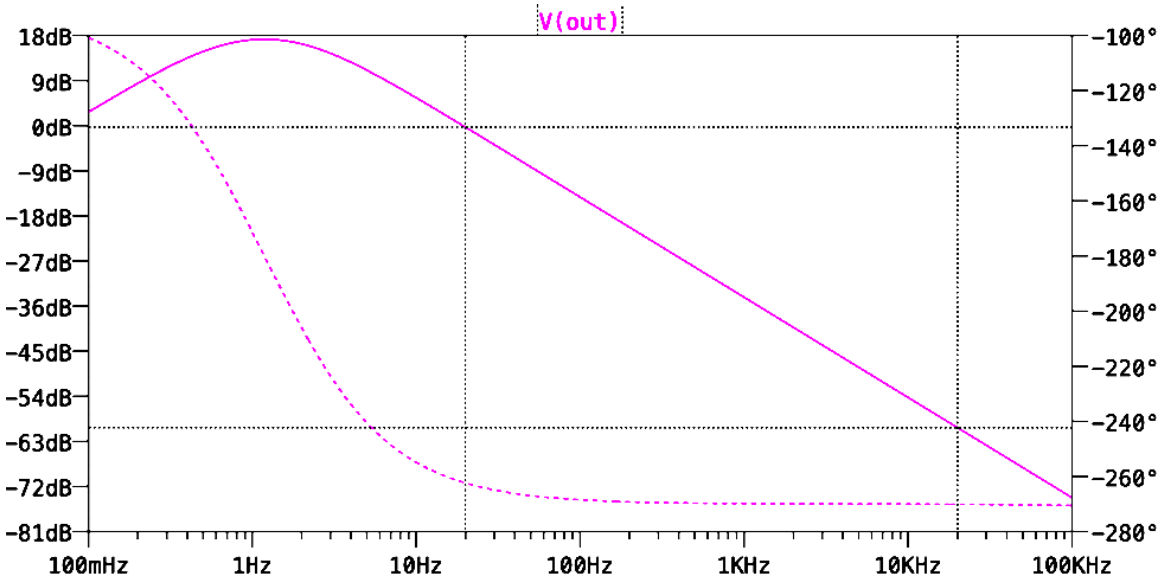

Figure 27: First Order Integrator Frequency Response

The plot shows a consistent -20dB/decade trend from 20Hz to 20kHz, indicative of a first order low pass filter or integrator. Unfortunately, there are limitations to this design in practical applications, explained as follows.

A -20dB/decade frequency response means higher frequency signals will become severely attenuated to the point of being inaudible. In theory this could be remedied by lowering the value of R2 to offset the magnitude response. Reducing the resistance value by a factor of 10 would create a 20dB offset to the magnitude response and reducing the resistance by a factor of 100 would create a 40dB offset. However, in the op-amp based design, the maximum peak to peak output voltage is limited by the op-amp rail voltages. Driving the op-amp beyond these values will cause the output voltage to saturate or phase reverse. In a 16V single supply system, the most optimal choice is to have the integrator outputting just below 16Vpp at 20Hz. This is shown in Figure 28(a). As the input frequency increases, the output attenuates at -20dB/decade; at 2kHz, the output voltage amplitude is 185mVpp, shown in Figure 28(b).

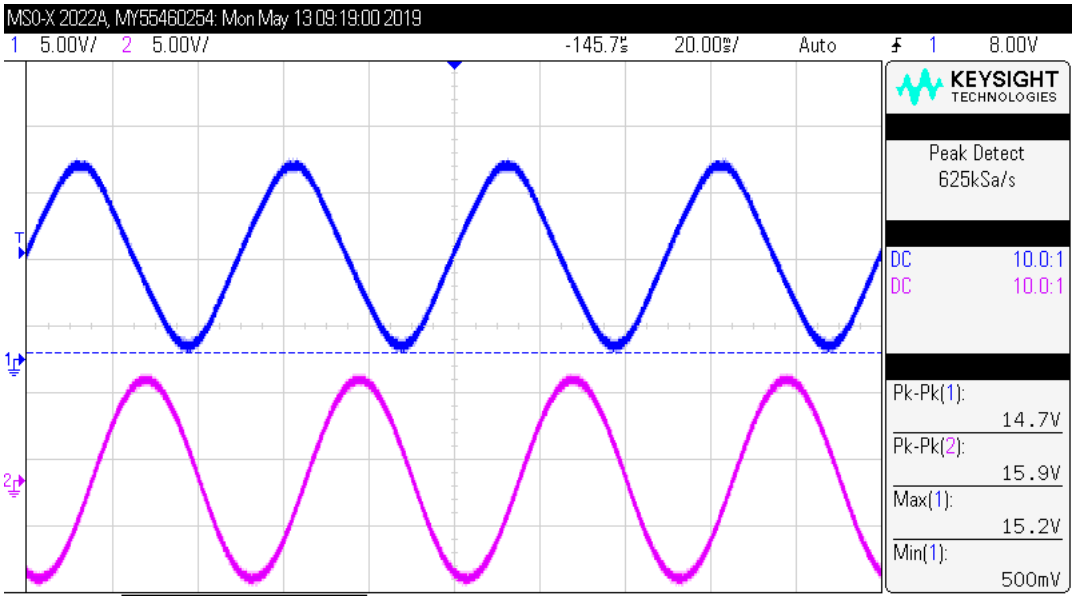

(a)

(b)

Figure 28: Input (Pink) and Output (Blue) Measured Waveforms for Fig. 24 Circuit. (a) 16Vpp Input at 20Hz. (b) 16Vpp Input at 2kHz

A voltage in the hundreds of millivolts range is too small to effectively modulate the pulse widths of the timer output signals. In addition, smaller input audio signals are more susceptible to noise contamination which will propagate throughout the rest of the system since it appears at the back end of the system. Thus, for some of the tests that are discussed in Chapter 5, the integrator is bypassed.

4.3 Audio Band Polyphase Filter

The purpose of the phase splitting network is to prepare the audio signal for SSB-PWM modulation. Much like SSB modulation, both the original and the Hilbert transform of the signal are used to modulate higher frequency carrier signals. The key difference is that traditional SSB-AM modulates the amplitude of sinusoidal waves, while this system modulates the pulse width of a square wave.

The desired phase splitting is accomplished with a polyphase filter which takes in two copies of the audio signal and outputs four signals, each being 90₀ out of phase with one another. Although the filter produces four output signals, only two signals with a relative phase of 90₀ are needed for the Pulse Width Modulators in the next block.

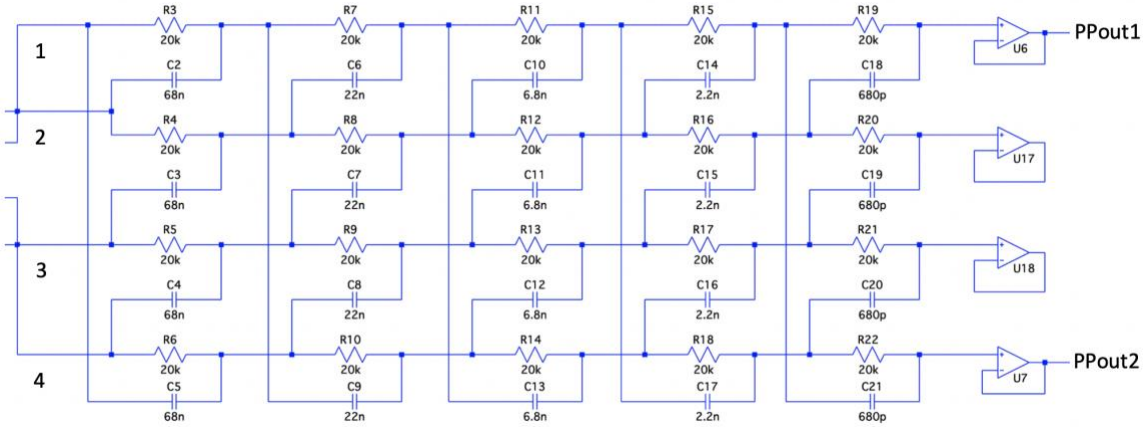

Figure 29: Five Stage Gingell Network Polyphase Filter

The topology shown in Figure 29 is a Gingell Network with five stages [21]. Each stage of the network is intended to create a sequence dependent filter with either a notch or a bandpass filter, centered at a specified frequency. The center frequency of every stage is calculated as

$$f_c = \frac{1}{2\pi RC} \tag{19}$$

For example, the first stage has R = 20kΩ and C = 68nF, resulting in a center frequency of f_{c1} = 117 Hz. Over the course of the five stages, the network creates passbands and notches that cover a significant portion of the audio frequency range. These frequencies are listed in Table 4.

Table 4: Gingell Network Center Frequencies

Stage	Center Frequency
1	117 Hz
2	362 Hz
3	1170 Hz
4	3260 Hz
5	11703 Hz

The first two input nodes are fed the same signal: a $6V_{pp}$ sinusoid with an 8V DC offset. Inputs 3 and 4 are fed an inverted version of this signal, creating an unbalanced input set similar to the one discussed in Section 2.3. Figure 30(a) shows the input waveforms in simulation. At the outputs, the four signals are balanced quadrature in a negative sequence: output 2 is -90_o out of phase from output 1, output 3 is -90_o out of phase from output 2, and output 4 is -90_o out of phase from output 3. Only output 1 and output 4 are used later on in the system, so they are renamed PPout1 and PPout2 as shown in Figure 29. The simulation results are shown in Figure 30(b), and the two waveforms PPout1 and PPout2 are shown on an oscilloscope in Figure 31.

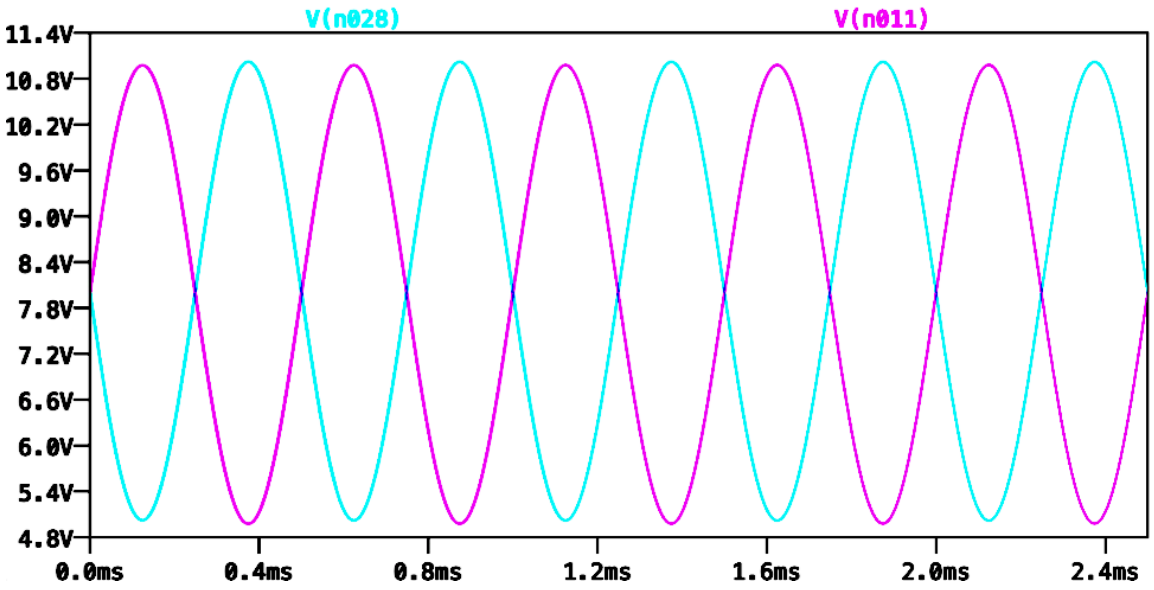

(a)

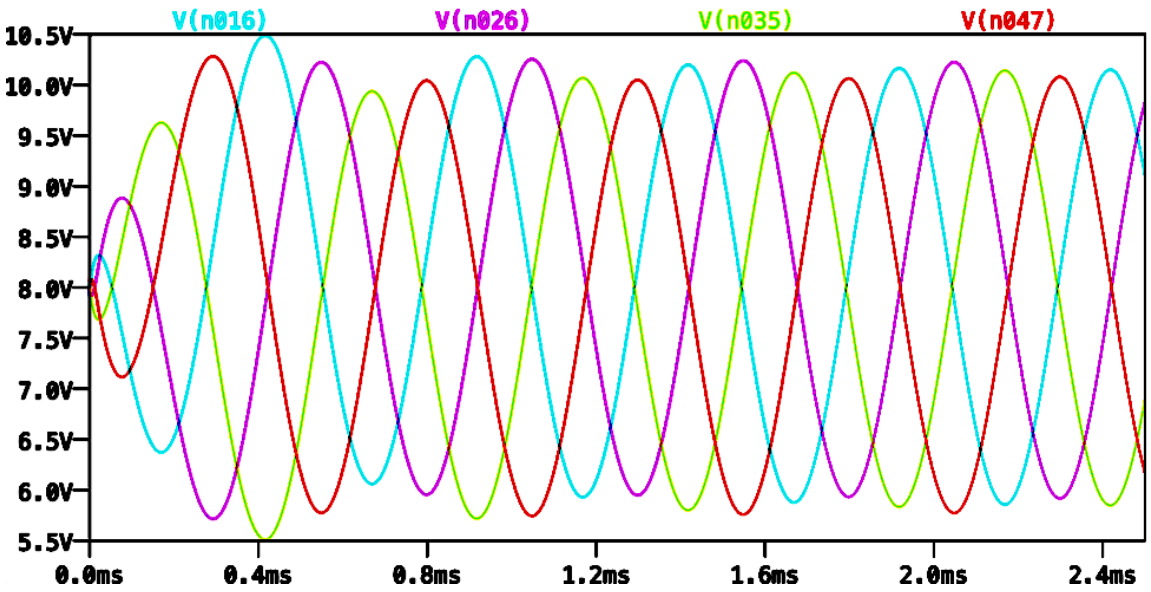

(b)

Figure 30: Polyphase Filter Simulation Input and Output Waveforms. (a): Inputs 1 and 3 (pink) and inputs 2 and 4 (cyan). (b): Outputs 1 (cyan), 2 (pink), 3 (green), 4 (red).

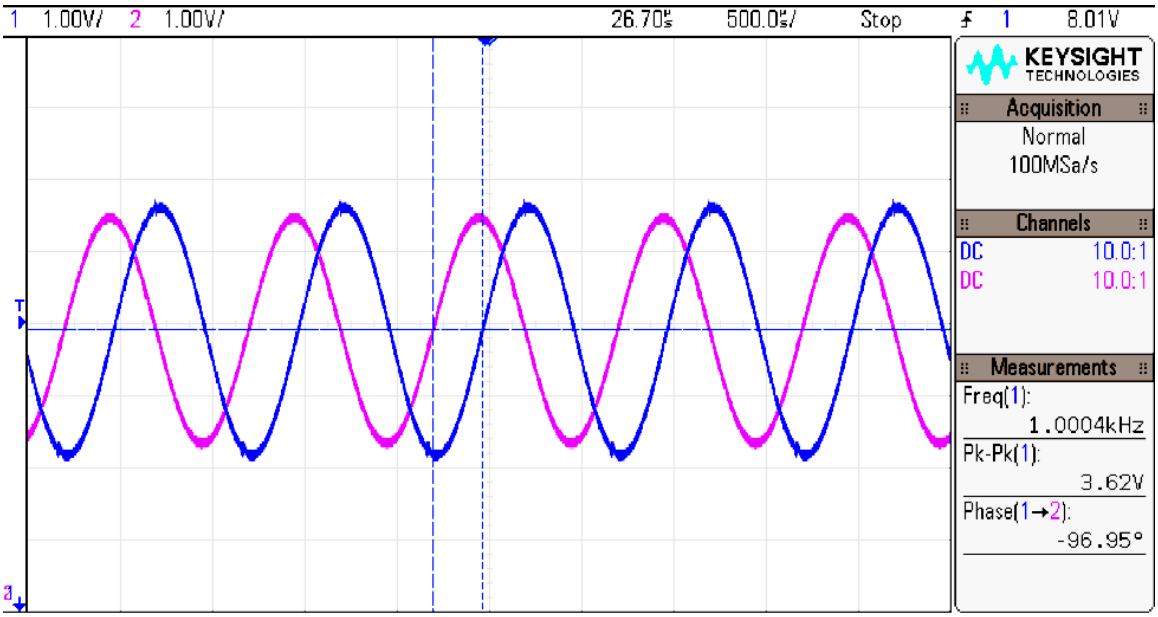

Figure 31: Polyphase Filter Outputs at 1kHz Input. PPout1 (Blue) and PPout2 (Pink)

4.4 40kHz Trigger Signal Generator

The trigger signal generator is a one-shot generator meant to create a pulse that is used as the trigger input for one of the Pulse Width Modulators. It is built using a 555 timer in monostable operation, with an RC network that controls the width of the generated pulse. The input to this subsystem is a 40 kHz square wave with a 50% duty cycle, labelled trig_I in Figure 32. The

output signal is labelled triq_Q. As their names imply, trig_I is used to generate the “I” PWM signal and trig_Q is used to generate the “Q” PWM signal in the Dual Pulse Width Modulators.

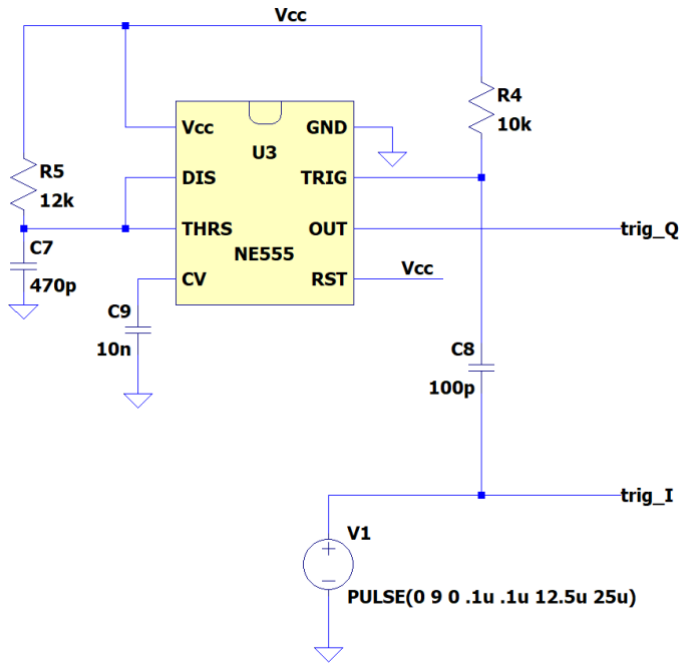

Figure 32: Trigger Signal Generator Circuit

On a downward edge of trig_I, the 100pF capacitor C8 will drop from Vcc until it reaches around $\frac{1}{3}Vcc$, which will cause the output of the 555 timer to go high. It will also cause the timer’s internal discharge device to turn off, preventing current flow into the discharge pin and allowing the 470pF C7 to charge via the 12kΩ resistor R5. These two component values create an RC time constant that allow the threshold pin voltage to reach $\frac{2}{3}Vcc$ after 6.25 microseconds, or a quarter cycle after the 40 kHz input signal goes low. This will cause a comparator output inside the timer to go high and drive the overall system output low. Simply put, the falling edge of trig_Q is designed to occur 6.25μs after the falling edge of the input. This result is shown in the oscilloscope capture in Figure 33.

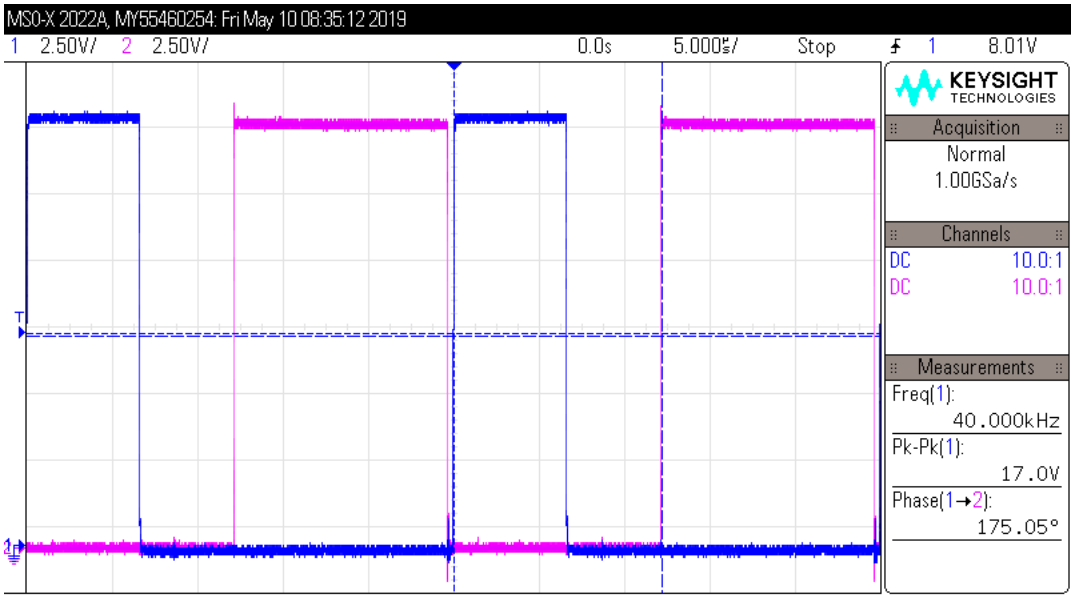

Figure 33: Trigger Signal Generator Input (Pink) and Output (Blue)

4.5 Dual One-Shot Pulse Width Modulators

This subsystem is responsible for encoding the two audio band signals into 40kHz ultrasonic PWM waveforms. It consists of two tunable current mirrors which set the idle duty cycle of the pulses, two 555 timers which modulate the audio signals into the pulses, and two passive trigger networks to control the incoming trigger input signals to the timers. The circuit diagram is shown in Figure 34.

The most important function of this system is to create two waveforms that can be summed to produce the desired SSB-PWM waveform. In order to do this, one timer is triggered with the trig_I signal, and the other timer is triggered with the triq_Q signal a quarter cycle later. In addition, the pulses are kept at a low duty cycle, below 25%, so that they can be summed together without having one signal overlap with the other. This “IQ-ing” and summing of the two outputs creates a similar effect to that of SSB modulation, where one double sideband amplitude modulated (DSB-AM) signal is added to a 90₀ out of phase DSB-AM signal to phase cancel one of the sidebands in the summed result. In this case however, instead of adding two DSB signals, the system adds two PWM signals to suppress the lower sideband and amplify the upper sideband. The spectrum appears around the fundamental frequency of the PWM waves, which is 40kHz.

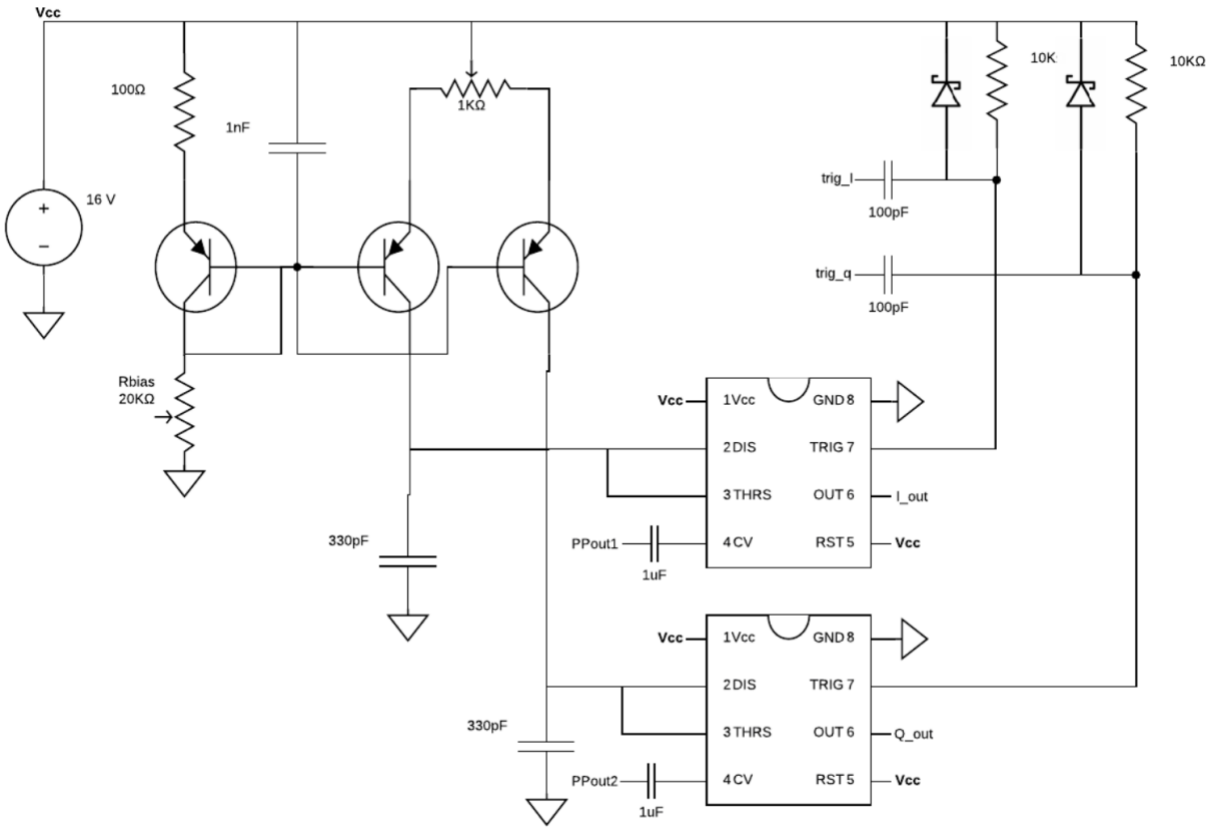

Figure 34: Dual One-Shot Pulse Width Modulators Circuit Diagram

Each timer generates a pulse that is initiated with a downward edge on the trigger input of the timer. This is controlled by the 40 kHz square wave trigger signal, either trig_I or trig_Q, fed into the trigger input via a passive trigger network. The trigger network consists of a 100pF capacitor, a Schottky diode, and a 10kΩ resistor. When the trigger signal goes low, it causes the timer's trigger pin voltage to momentarily fall below $\frac{1}{3}Vcc$ and initiate the output pulse while the 100pF capacitor begins to recharge to V_{cc} via the 10kΩ resistor. With the output pulse high, the base voltage of the 555 timer's internal discharge transistor goes low, causing the transistor to inactivate and allowing the 330pF capacitor to charge. As shown in Figure 34, the 330pF capacitor holds the voltage at the threshold pin, and it is charged via a current mirror. The 10kΩ potentiometer R_{bias} is tuned to control the current flowing from the mirror into the capacitor. The 1kΩ potentiometer between the two current sources is tuned to account for component mismatch between the two branches and ensure an equal amount of current flows between them. The capacitor will charge linearly until it exceeds a threshold voltage, upon which the output will go low and the pulse will be complete.

With this information, a formula to determine the required current is derived, starting with the equation for the current flowing through a capacitor $i_c = C\frac{dV}{dt}$. Given the current is a constant, the equation can be rewritten as

$$i_c = C\frac{\Delta V}{\Delta t} \tag{20}$$

where ΔV is the threshold voltage, which equals $\frac{2}{3}Vcc = \frac{2}{3}(16) = 10.67\ V$ when no input is applied to the Control Voltage (CV) pin of the timer. Δt is the time it takes for the capacitor to charge up to the threshold voltage, which is also the pulse duration. This system is designed for a no input duty cycle of 16%, which means the idle pulse duration can be calculated.

$$\Delta t_{idle} = 16\% * \frac{1}{40000\ Hz} = 4\mu sec$$

Finally, the values for C, ΔV, and Δt are plugged in to Equation 20 and i_c is determined to be

$$i_c = 330pF\,\frac{10.67V}{4\mu sec} = 0.88mA$$

With an audio input capacitively coupled to the CV pin, the threshold voltage becomes $\frac{2}{3}Vcc + PPout1$ or $\frac{2}{3}Vcc + PPout2$ depending on the timer. As the audio signal changes strength it will cause the threshold voltage to move, which will affect the amount of time it takes for the capacitor to charge up to the threshold. This mechanism is what controls the pulse width and thus the duty cycle of the output as it is linearly modulated by the input audio signal. The 330pF capacitor voltage is shown along with the corresponding pulse in Figure 35.

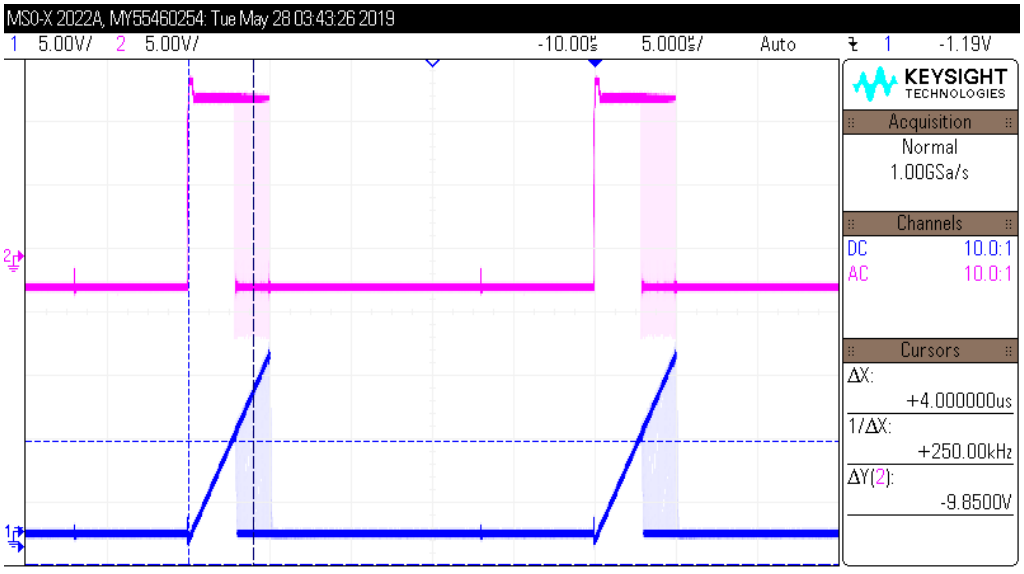

Figure 35: 330pF Capacitor Voltage (Blue) and Corresponding PWM Wave in Dual Pulse Width Modulator Sub-circuit.

In this oscilloscope capture the pulses are rapidly changing duty cycle based on the timer threshold voltage. It is worth noting that the maximum threshold voltage is the supply voltage V_{cc}. By this, the peak voltage at the CV pin of the timer is calculated.

$$\frac{2}{3}Vcc + PPout1_{peak} = Vcc \tag{21}$$

$$PPout1_{peak} = \frac{1}{3}Vcc = 5.33V$$

The peak pulse duration can also be calculated as $\frac{3}{2}\Delta t_{idle} = 6\mu sec$. Assuming the input audio signal has symmetric voltage swing from DC, the minimum pulse duration is 2μsec. This translates to a duty cycle range of 8% - 24%, which meets the system requirements of remaining below 25%.

Figure 36 shows the two idle pulses coming from both timers, spaced around a quarter cycle or 6.25μsec from each other to prevent overlapping signals. The waveforms can now be summed together.

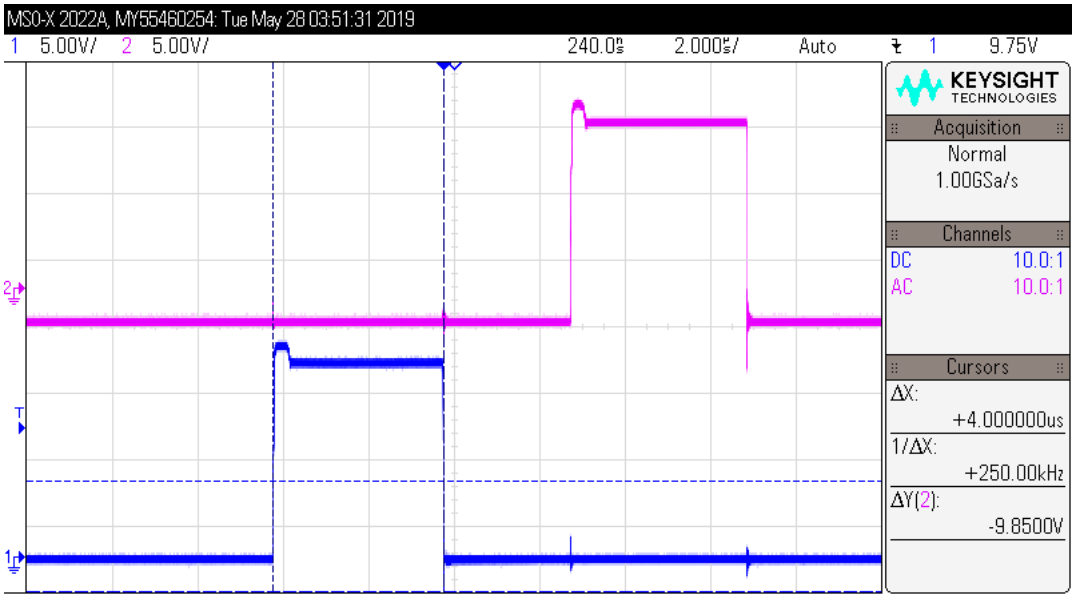

Figure 36: Dual Pulse Width Modulator Idle Output Waves. I Output (Blue) and Q Output (Pink)

4.6 Wired-OR Voltage Summer

This part of the system is meant to combine the outputs from the two Pulse Width Modulators into a single waveform. The sub-circuit is shown in Figure 37, which consists of two diodes and a 10kΩ pull-down resistor. When the output from one of the modulators Iout is high, the diode D1 activates and the pulse appears at the node labelled Vout. Likewise, when Qout goes high, D2 activates and that pulse appears at Vout. This design is viable because Iout and Qout are never active at the same time, and thus the diode based OR will behave like a summing block.

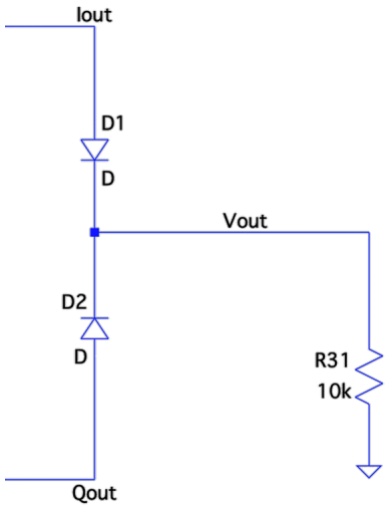

Figure 37: Wired OR (Voltage Summer)

4.7 TC4427AEPA MOSFET Switching Amplifier

The final subsystem is a high-speed power MOSFET amplifier which is used to drive the transducer array. This circuit takes in the composite output signal from the wired OR and produces a clean $16V_{pp}$ switching waveform, shown in Figure 38.

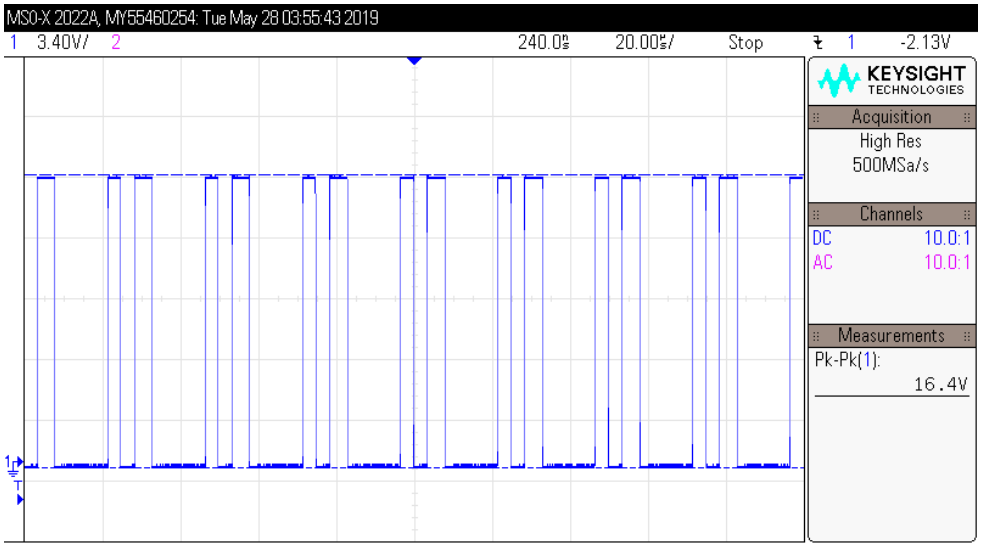

Figure 38: MOSFET Switching Amplifier Output Waveform

It has a high output current capability of 1.5A which is necessary to provide current to 25 transducers. In Section 3.2 on the transducer impedance, at 40kHz each transducer has an impedance of about 860Ω based on Figure 18. With 25 transducers in parallel, the overall impedance becomes $\frac{860}{25} = 34.4\Omega$. By Ohm's Law, the current needed to drive the transducers is calculated.

$$I_{drive} = \frac{V_{drive}}{Z_{load}} = \frac{16V}{34.4\Omega} = 465mA \tag{22}$$

4.8 Ultrasonic Transducer Array

The transducer array emits the ultrasonic signal into the air, which will travel and demodulate to produce audio waves. 25 transducers are placed in parallel in a 5x5 grid. This can be seen in the full system image in Figure 39. The transducers are spaced 10mm away from each other horizontally and vertically, center to center, but 14.14mm diagonally. Ideally all the transducers should be placed such that the distance between their centers is equal to their diameters, so the waves constructively interfere [7]. So, the spacing is not ideal, but it does maximize the number of transducers that could fit on the perf board within the spatial limitations.

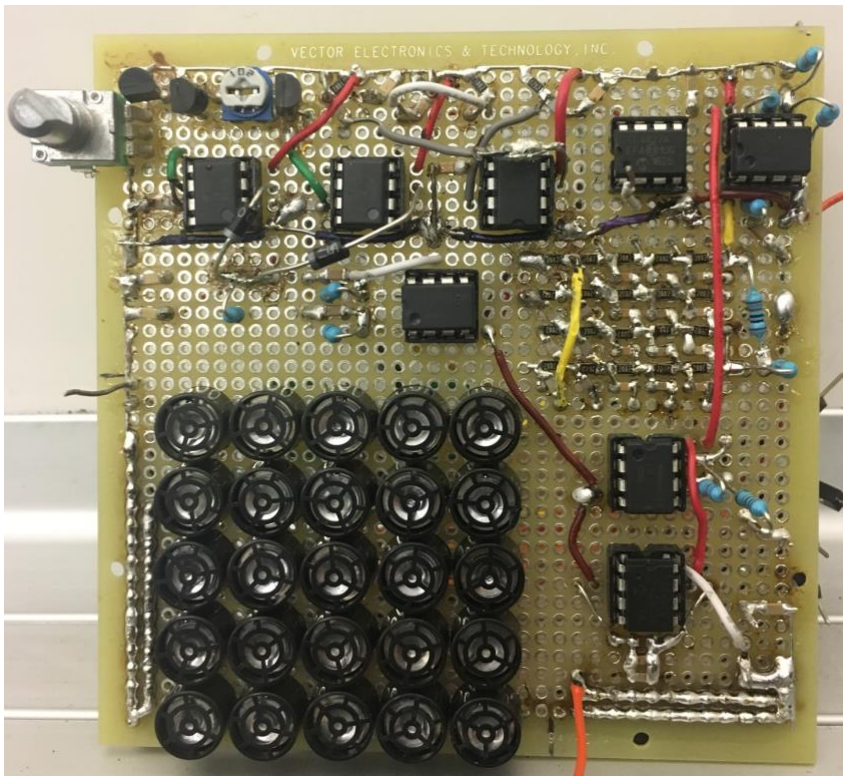

Figure 39: Full System in Hardware Image. 5x5 Transducer Array in Bottom Left Corner.

The wiring of the array is shown on the reverse side in Figure 40. All the negative (-) pins of the transducers are shorted together and soldered to the common ground node of the system. The positive pins, however, are connected via jumper cables to a jumper array which is connected directly to the output of the MOSFET Driver. This allows for the transducers to be conveniently connected and disconnected as needed for testing.

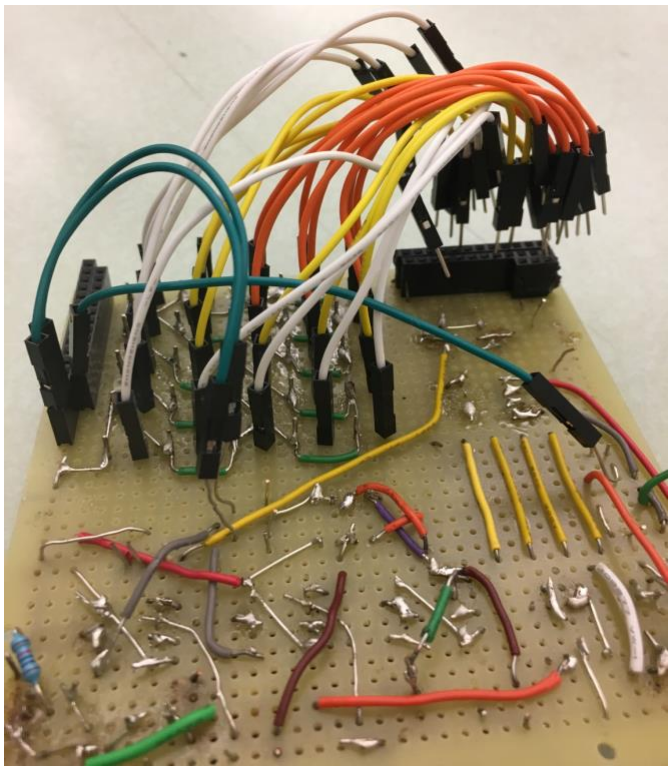

Figure 40: Full System in Hardware Reverse Side. Transducers Connected Via Jumper Cables to Jumper Array.

Unfortunately, upon connecting a single transducer to the system, the output waveform began to distort with a consistent high frequency ringing around 320kHz. This issue remained unresolved and will be discussed in greater detail in Chapter 5.

Chapter 5

TESTS AND RESULTS

5.1 Full System Open Load Test

To verify the validity of the dual PWM system, a single tone test is done to see whether or not the output signal has a single sideband spectrum. For this test, the output is measured with no load connected so that the signal does not experience any resonance effects from the transducers. This also means the first order integrator is omitted because the output will not enter the air and demodulate as per Berktay's equation. A simple diagram of the test setup is shown in Figure 41, where $A*\sin(\omega_m t)$ is the input tone and V_{out} is the SSB-PWM signal.

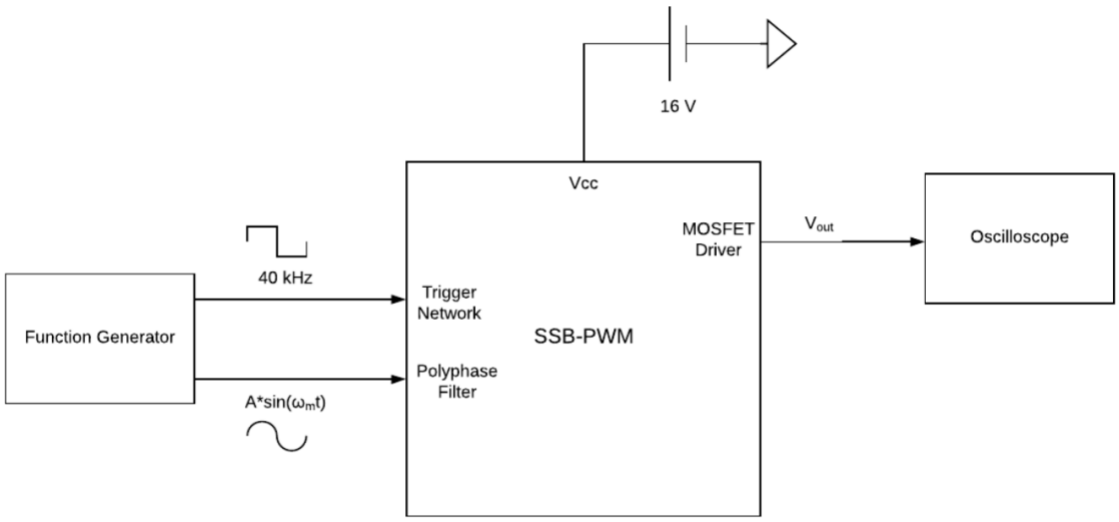

Figure 41: Full System Hardware Test Setup

The input signal frequency is incrementally increased from 1kHz to 20kHz to cover the audio bandwidth. The output is measured with an oscilloscope and the FFT is taken using the "Math" operation on the oscilloscope to show the frequency content of the signal. Figure 42 shows the output FFT on the scope display for a 2kHz input signal, highlighting the difference in levels between the upper sideband (USB) and lower sideband (LSB) in the output signal. Figure 43 plots the USB and the LSB magnitudes over the audio spectrum on the same plot to compare the difference.

Figure 42: FFT of the System Output Signal V_{out}. Input Voltage $V_{in} = A*\sin(2\pi*f_m*t)$

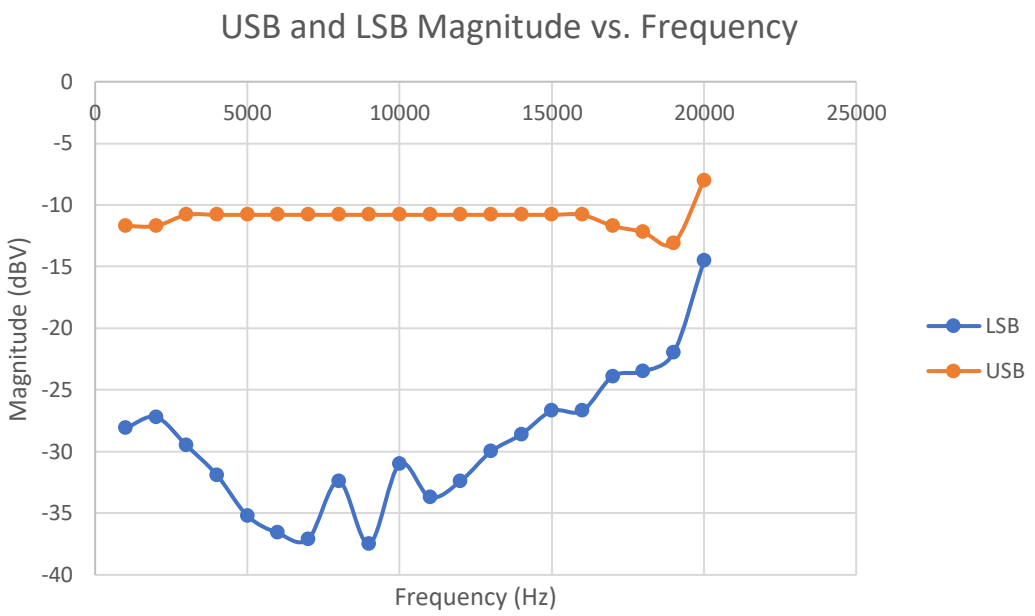

Figure 43: Comparing the Magnitudes of the Upper and Lower Sidebands in the No Load Output Signal of the SSB-PWM System

As the trendlines indicate from around 3kHz to 13kHz, the system has >20dB difference between the USB and LSB levels. This shows the legitimacy of using PWM signals to create an SSB-AM waveform.

5.2 Simulating Nonlinear Demodulation

Unfortunately, the final hardware design is unable to produce recordable audio. In a qualitative music play test, the lower frequency content is heavily distorted and therefore has to be kept at a lower level to minimize the THD. Higher frequency content is more recognizable but is too quiet to record with a practical microphone setup. Instead, the demodulation process is simulated in LTSpice to facilitate some testing for harmonic distortion in the demodulated audio signal.

The model for demodulation is based on creating the effect of Berktay's equation, where the demodulated signal is proportional to the square of the output signal's envelope function. It was used initially in a modulation scheme known as recursive single sideband modulation (RSSB) to develop a distortion model in the preprocessing segment and use that information to reduce overall distortion [23]. The nonlinear demodulator block diagram is shown in Figure 44.

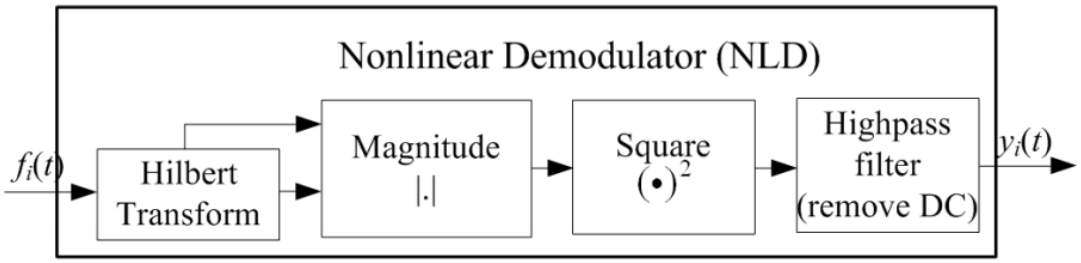

Figure 44: Nonlinear Demodulator Block Diagram [2010_Ji, Gan, Tan, Yang]

The Hilbert Transform, magnitude operator, and square operators are used to take the envelope squared of an SSB-AM signal. As outlined in Chapter 2, the envelope of an SSB-AM is computed by taking the analytic SSB signal and finding its magnitude. In the SSB-PWM case, even though it is a two-level signal without an "envelope," the nonlinear demodulator can still be used provided the narrowband transducer array is included to filter out the higher order PWM harmonics before applying the Hilbert Transform. Notice there is no double differentiator in diagram above, because this model does not account for the effects of a double integration from the preprocessing block and the narrowband transducer. For our simulation, the transducer representation is included in the form of passive components, and thus a single differentiator is also included. The simulation circuit is shown in Figure 45.

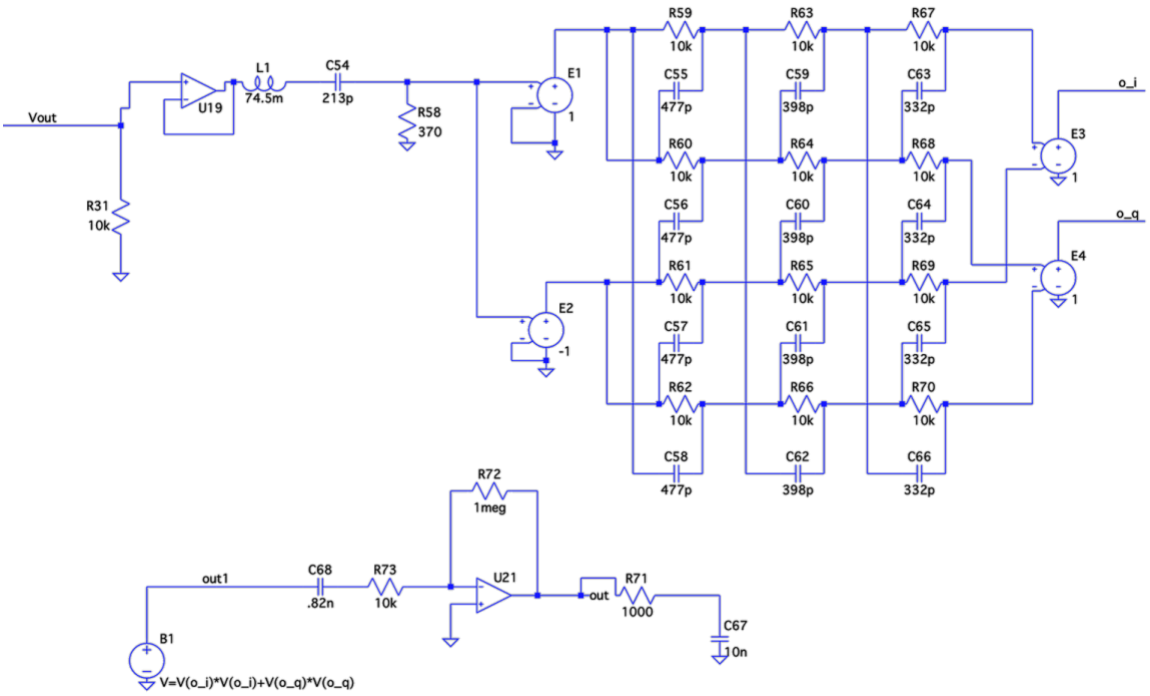

Figure 45: Nonlinear Demodulation Simulation Circuit Diagram

The driving signal “Vout” first passes through the transducer model made of the same inductor, capacitor, and resistor values that were used to define the ultrasonic transducer impedance in Table 1. The three-stage polyphase filter has center frequencies at 33.4kHz, 40kHz, and 47.9kHz, around the carrier value of 40kHz, and performs the Hilbert transform to separate out the real and imaginary components of the PWM signal “envelope.” The outputs of the polyphase filter are used in the governing equation for the behavioral voltage source B1, which has the voltage $V = V(o\_i)^2 + V(o\_q)^2$. This represents the “envelope squared” of the driving signal. Finally, an op-amp based differentiator creates the effect of a single derivative on the simulated output audio signal.

The demodulator is first tested using a two-tone test on the demodulator alone to represent normal SSB AM. Two signals of equal magnitude at 40.3kHz and 41.3kHz drive the system and the output of the demodulator produces the envelope squared function, which in this case is the difference frequency of the signals. Figure 46 shows the input ultrasonic signal and the output waveform on the same plot. A successful 1kHz signal retrieval indicates that the demodulator simulation is functional. Now the full dual PWM system can be tested with the demodulator to study the distortion of the produced audio.

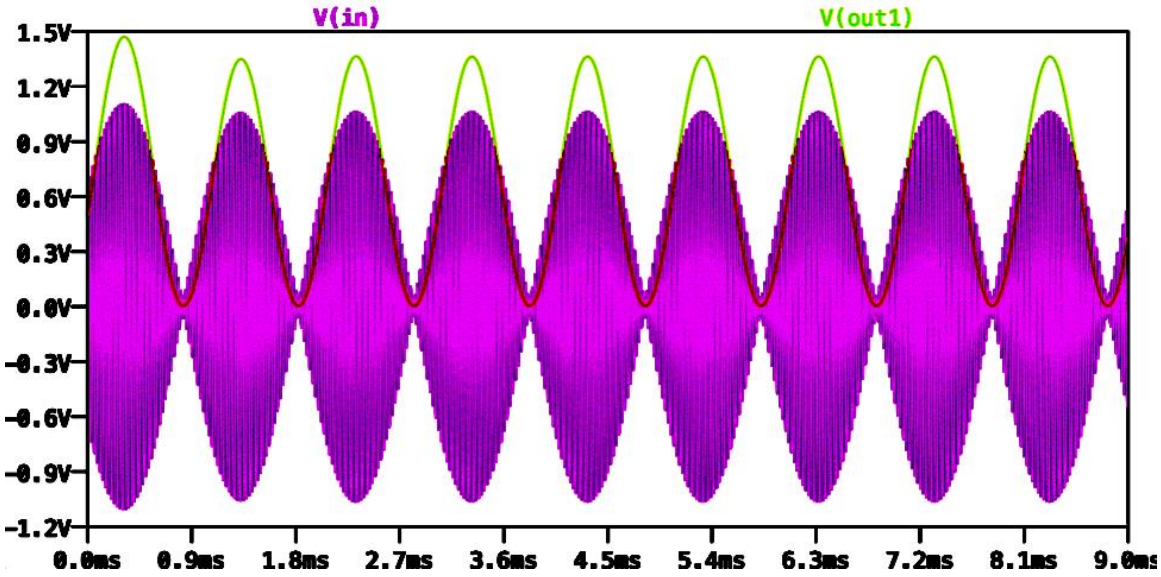

Figure 46: Nonlinear Demodulator Test Simulation Waveform. Two Tone Ultrasonic Input (Pink) and Demodulated Output Signal (Green).

The first test is a single sinusoidal input with increasing magnitude to establish a relationship between the input level and the output distortion. The input is incremented from 1Vp up to 6Vp, and the test is done for a 500Hz, 1kHz, 2kHz, and 4kHz signal. The plots in Figure 47 show the results of the test. Each trendline represents a different frequency and the Total Harmonic Distortion is computed using the Fourier analysis command in LTSpice.

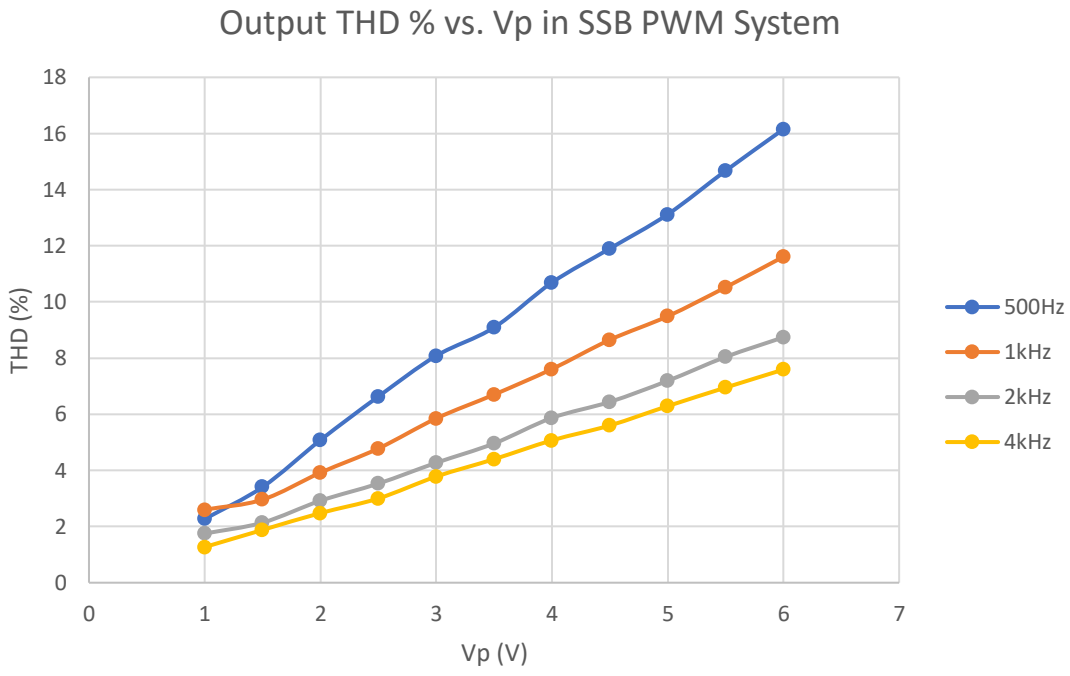

Figure 47: Single Tone Test Results for Total Harmonic Distortion in Simulated SSB-PWM System

Based on the results, there is a clear linear relationship between the input peak voltage V_p and the output THD. For the 500Hz case the relationship is the most severe, and the slope gradually decreases as the frequency increases. This is consistent with the previous literature mentioning the difficulty of reproducing lower frequencies due to higher distortion. Figure 48 below shows a retrieved 1kHz squared envelope signal with its corresponding ultrasonic SSB-PWM waveform.

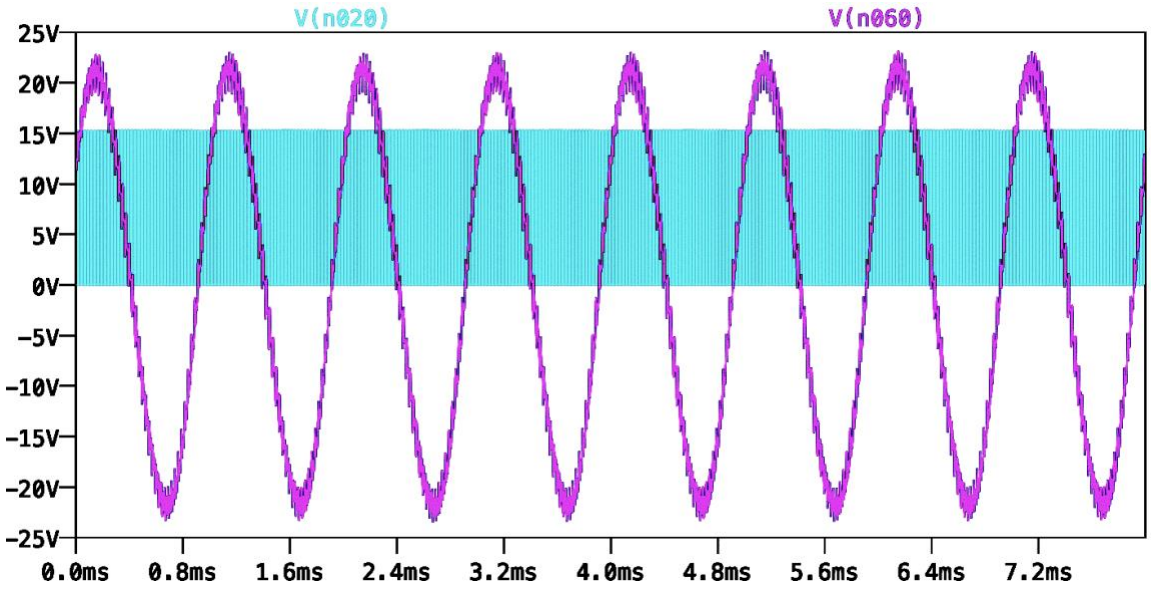

Figure 48: Single Tone Test for Simulated SSB-PWM with Nonlinear Demodulation. SSB-PWM Output (Cyan) and Demodulated 1kHz Input Tone (Pink)

For the next test, two tones are applied to the input of the system, and the output is examined for intermodulation distortion. The hypothesis is that with two tones and a carrier, the nonlinear demodulation will cause energy to appear at the difference frequency of the two tones. For example, if a 400Hz and 600Hz tone are used as inputs, the demodulation process will cause a third tone to appear at 600 – 400 = 200Hz. This distortion term is known as 2_{nd} order intermodulation or IMD2.

Table 5: Two Tone Test for Intermodulation Distortion at 200Hz.

Input Tone Frequencies	**IMD2**
400Hz and 600Hz	1.51%
900Hz and 1.1kHz	1.68%
1.9kHz and 2.1kHz	2.26%
3.9kHz and 4.1kHz	4.00%

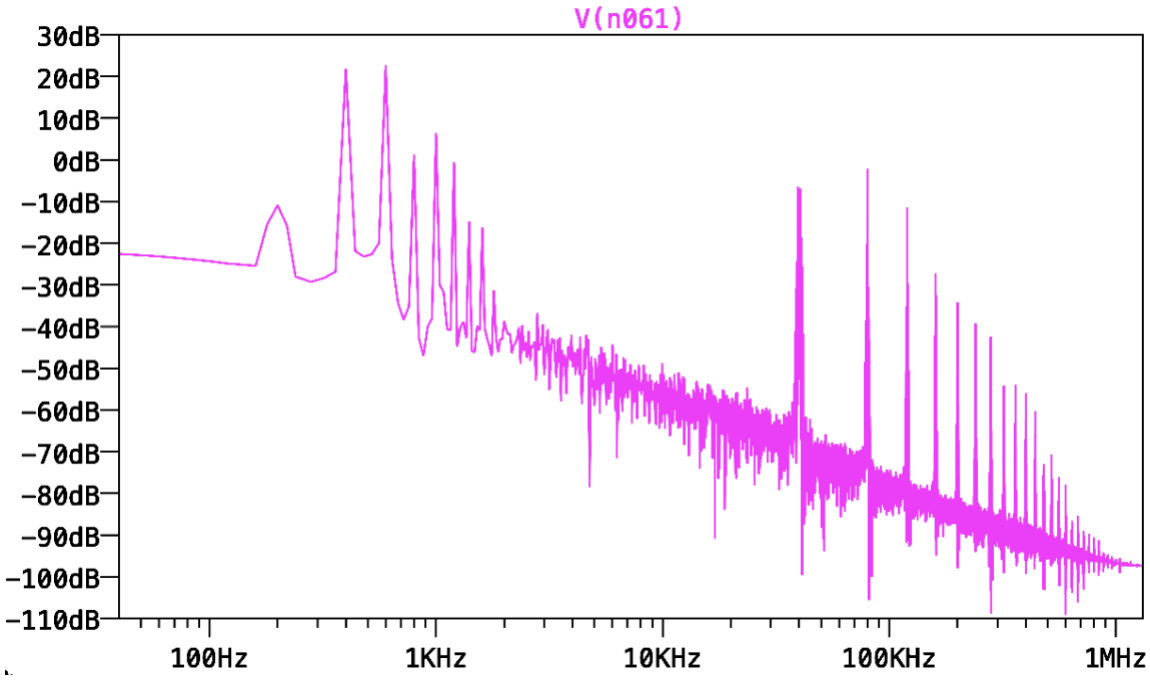

Figure 49: FFT of Demodulated Signal in Two Tone Test Simulation with Inputs at Frequencies 400Hz and 600Hz

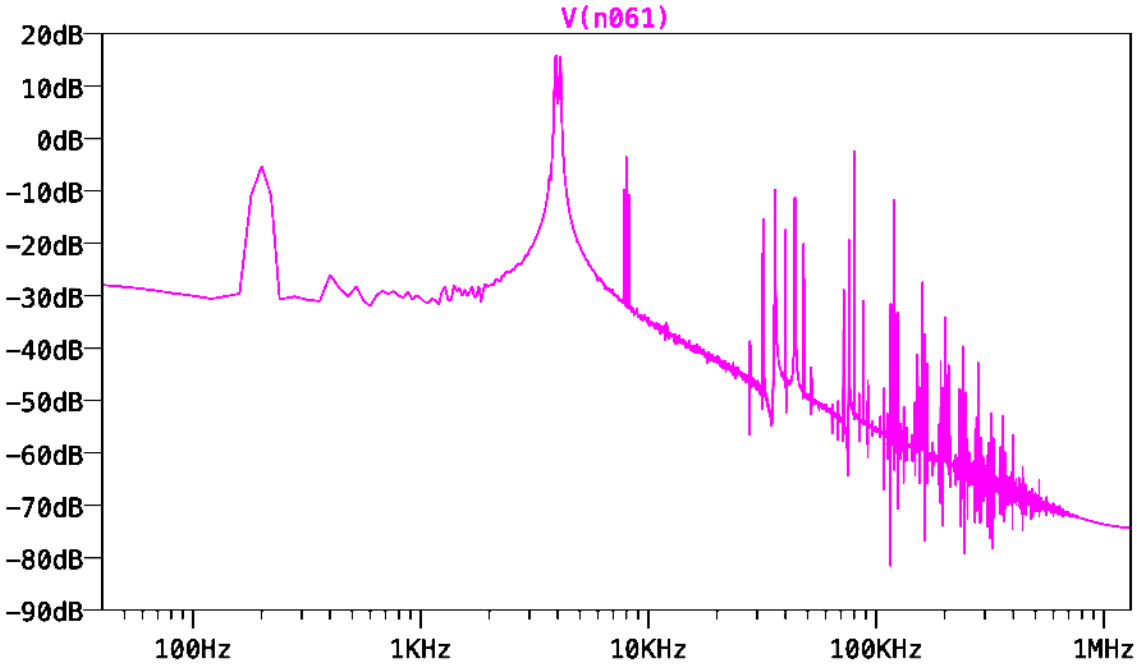

Figure 50: FFT of Demodulated Signal in Two Tone Test with Inputs at Frequencies 3.9kHz and 4.1kHz

5.3 Op-amp Crossover Distortion in AC Coupled Sub-circuits

The LM358 op-amp is used in and between several stages of the system, usually as an output buffer or inverter. For example, the output of the integrator is buffered before driving two inputs of the polyphase filter and inverted before driving the other two inputs of the polyphase filter. This is shown in Figure 51 with the op-amps labelled U1 and U2.

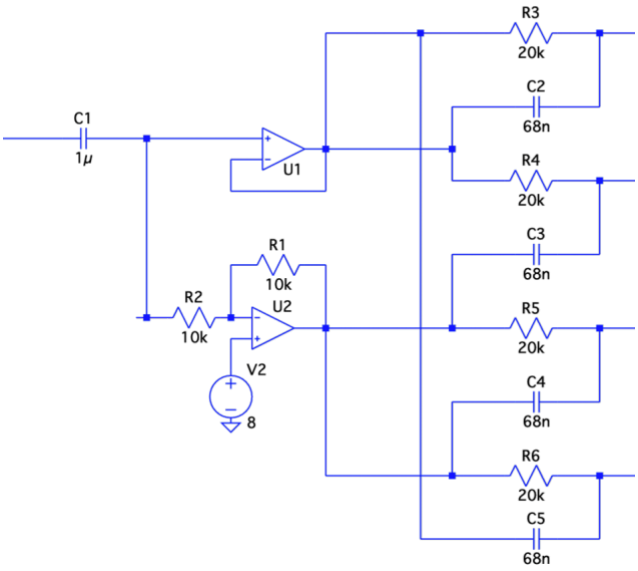

Figure 51: Op-amp Buffer and Inverter Driving Polyphase Filter

Notice both op-amps are directly connected to the capacitors C2, C3, C4, and C5, meaning there is some AC coupling happening between the op-amp outputs and the polyphase network. When an op-amp is AC coupled to a load, and the output voltage swings above and below the load's reference point, a phenomenon known as crossover distortion can occur [24]. This happens because the op-amp output stage needs to alternatively switch between supplying and drawing current, and the switching mechanism creates a glitch in the output signal. Observe the op-amp schematic in Figure 52.

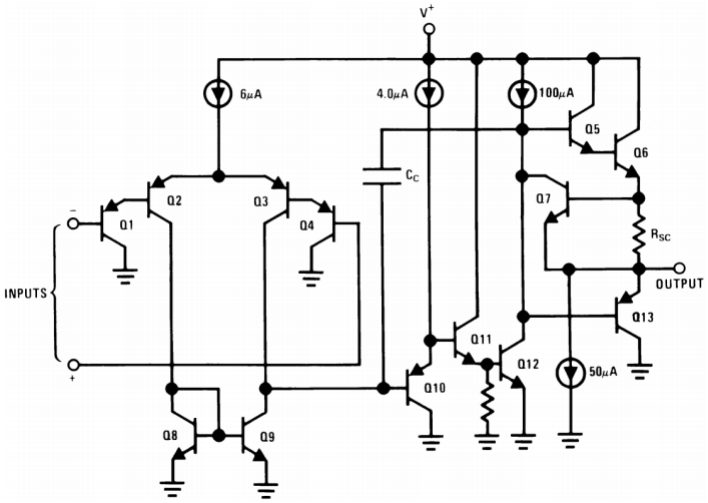

Figure 52: LM358 Op-amp Schematic Diagram

The NPN transistor Q12 is actively loaded to drive the output transistors Q6 and Q13. Since Q6 is an NPN transistor and Q13 is a PNP transistor, the two cannot be on at the same time. When the output needs to source current the collector voltage of Q12 rises and turns on Q5 and Q6. When the output needs to sink current the collector voltage drops and turns on Q13. The time it takes to switch from one biasing condition to the other is limited by the internal compensation capacitor C_C, which means there is a finite period where neither transistor is on. During this period the output voltage is floating, and that creates the glitch in the overall waveform. The effects are clearly seen in the output of the polyphase filter in Figure 53 for a 10kHz input.

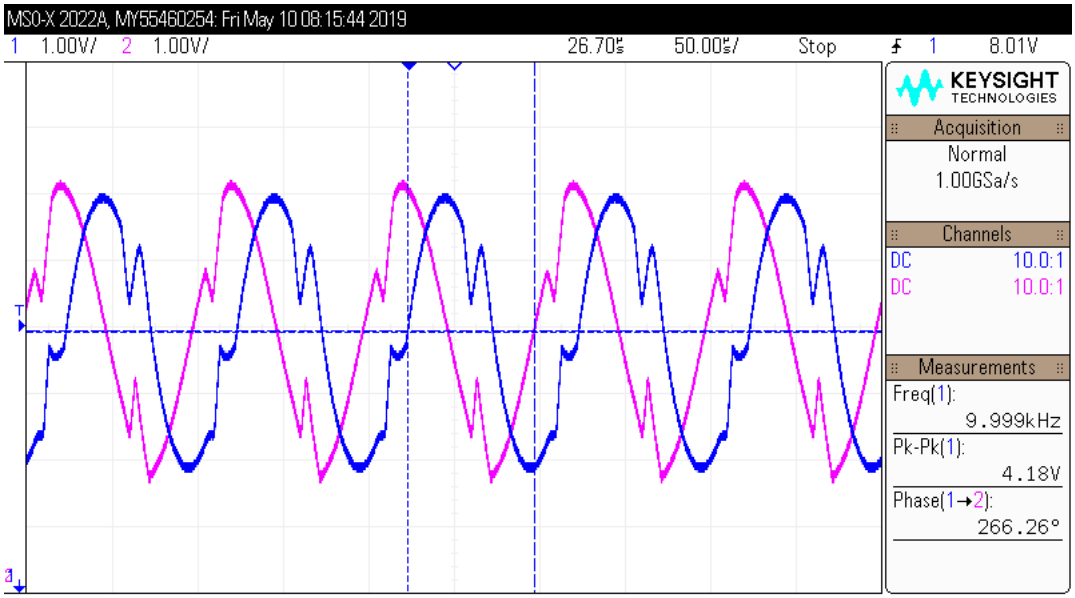

Figure 53: Crossover Distortion in Polyphase Filter Output with 10kHz Input Signal

The solution to this issue is to add a pulldown resistor to ground from the output of the op-amp. This ensures the NPN transistors Q5 and Q6 can continuously source current into the resistor and prevent the output from crossing over. The schematic in Figure 54 shows a simplified version of the op-amp buffer circuit with a 1KΩ pulldown resistor. The resistor value should be small enough such that both the output and the load can source current into the resistor.

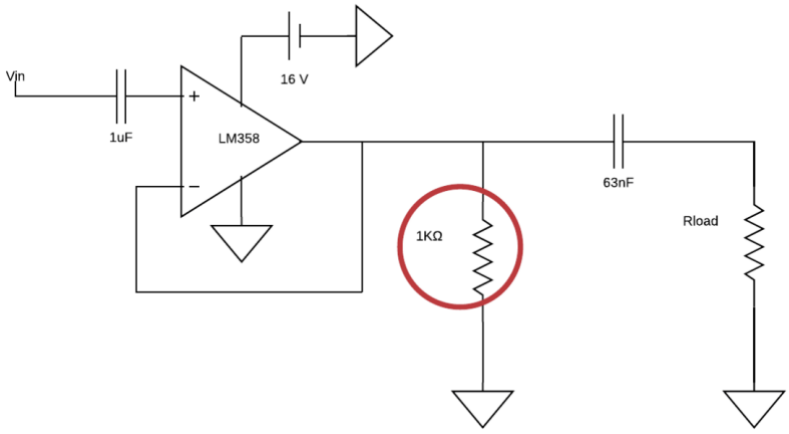

Figure 54: Crossover Distortion Correction With 1kΩ Pulldown Resistor

The results of the correction are shown in the oscilloscope images of the polyphase filter output in Figure 55.

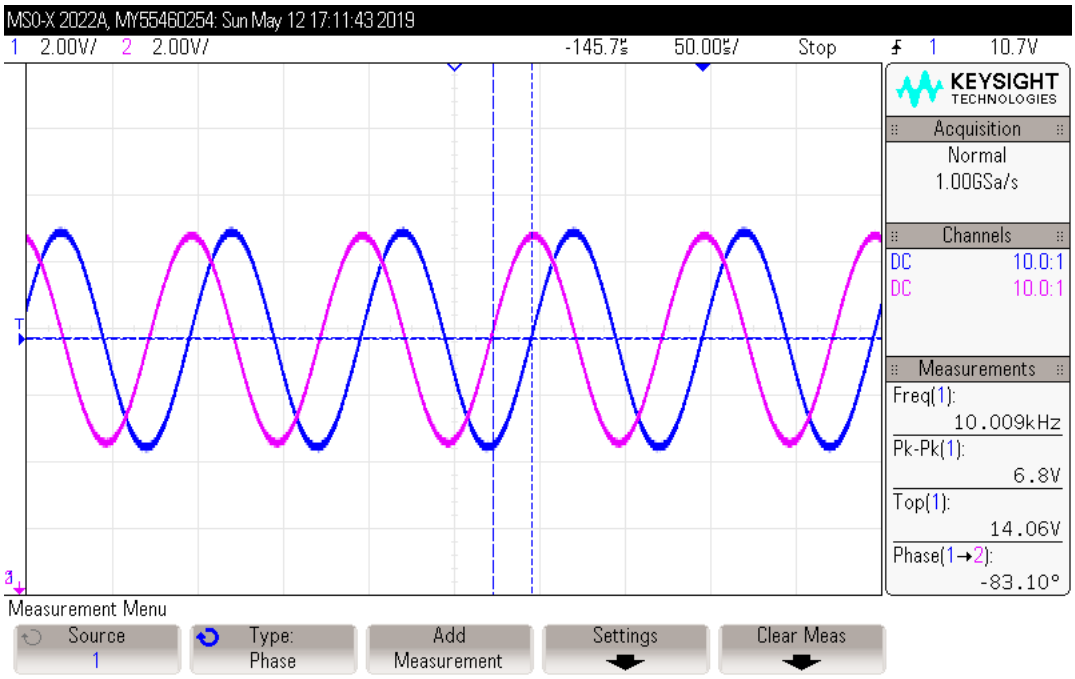

Figure 55: Corrected Polyphase Filter Output with 10kHz Input

5.4 Switching Noise in 555 Timers

Another abnormality occurs within the two LM555 timer ICs, where the trigger inputs trig_I and trig_Q affect the input signal at the Control Voltage pins. Each time there is a rising or falling edge of the trigger signals, the sudden change in voltage propagates through the IC and creates “switching noise” in the circuit. This is reflected in the two audio frequency signals shown in Figure 56, where the waveforms are clearly corrupted with spikes in voltage at the rate of the trigger signals.

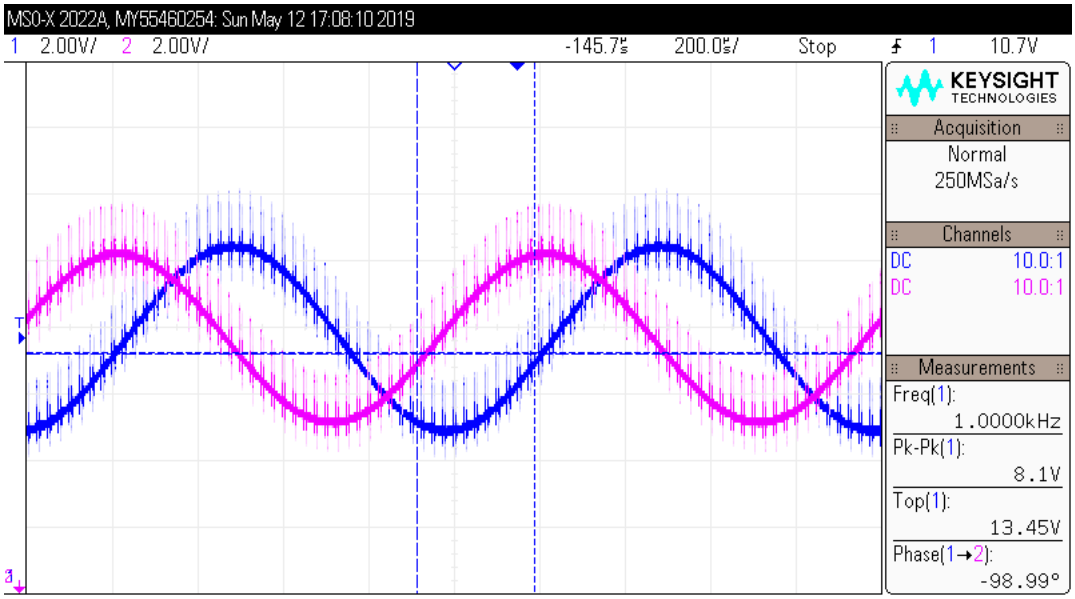

Figure 56: Switching Noise on the Control Voltage Input Pins of the 555 Timers

Observing the waveforms over a shorter time period in Figure 57, the voltage transients have a nearly identical pattern on both waveforms, even though the incoming trigger signals are different for the two timers. This would suggest that the switching noise is propagating through some common node between the two timers. The supply and ground nodes are only common points of connection between the two timers, so it is possible there is ground looping at play. Another place where crosstalk may be happening is the output of the two timers, since they are wired together via diodes. This is unlikely however because the signal would have to drive the diodes beyond their breakdown voltages.

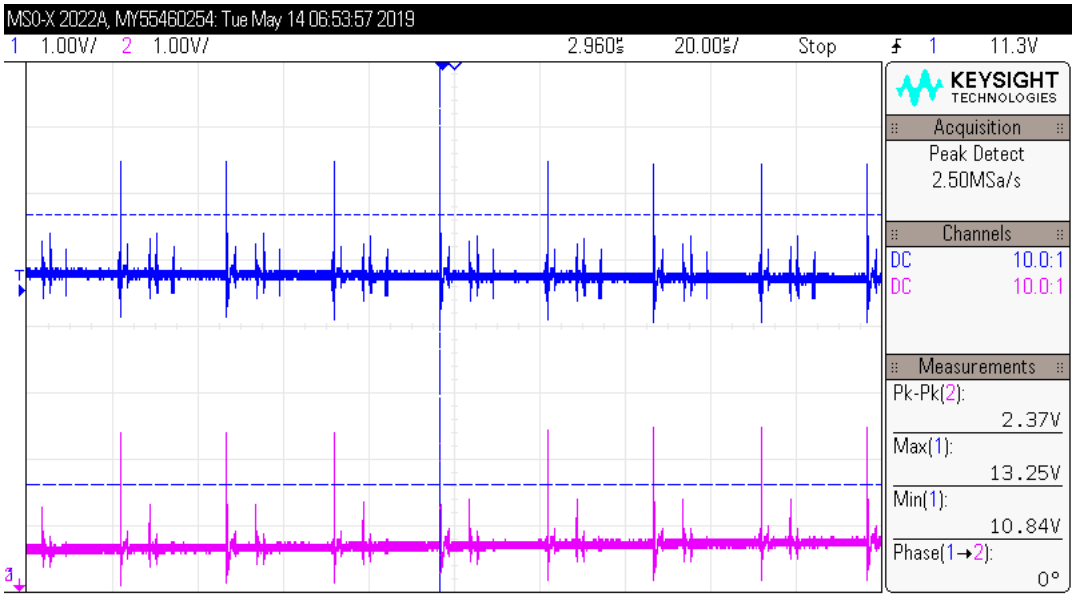

Figure 57: Switching Noise is Common to Both 555 Timers

It does seem clear that the switching noise is not coming directly from the trigger generator itself, because that would create two unique noise patterns in the audio signal inputs. In Figure 58(a) and (b), one of the CV waveforms is compared to the two trigger signals. There are two instances where one of the trigger signals switches, and this creates two small noise signatures. There is also one instance where the I trigger signal falls and the Q trigger signal rises at the same time, and this creates a larger noise signature in the CV waveform. In essence, both trigger signals affect both the CV signals.

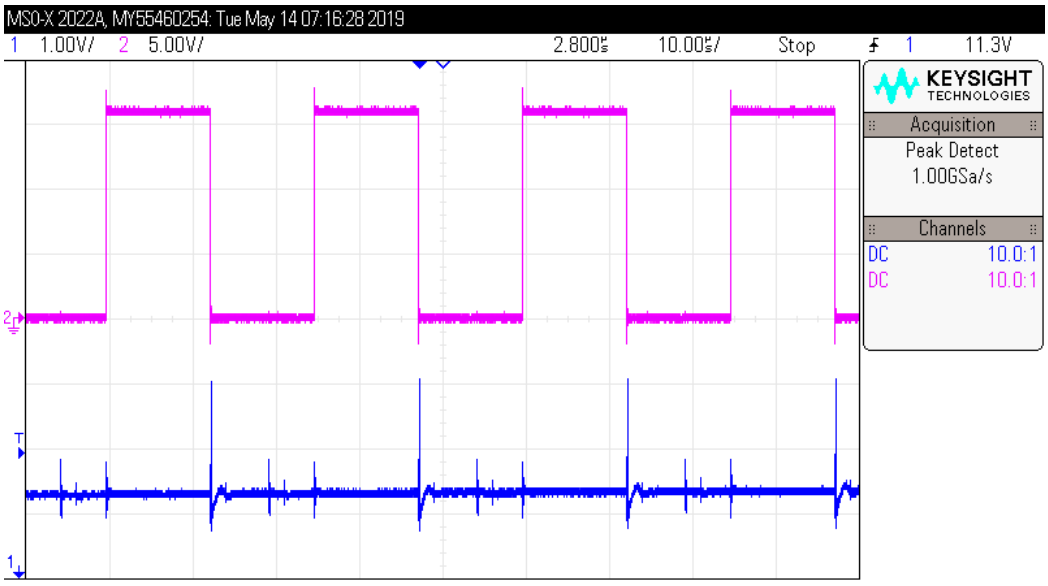

(a)

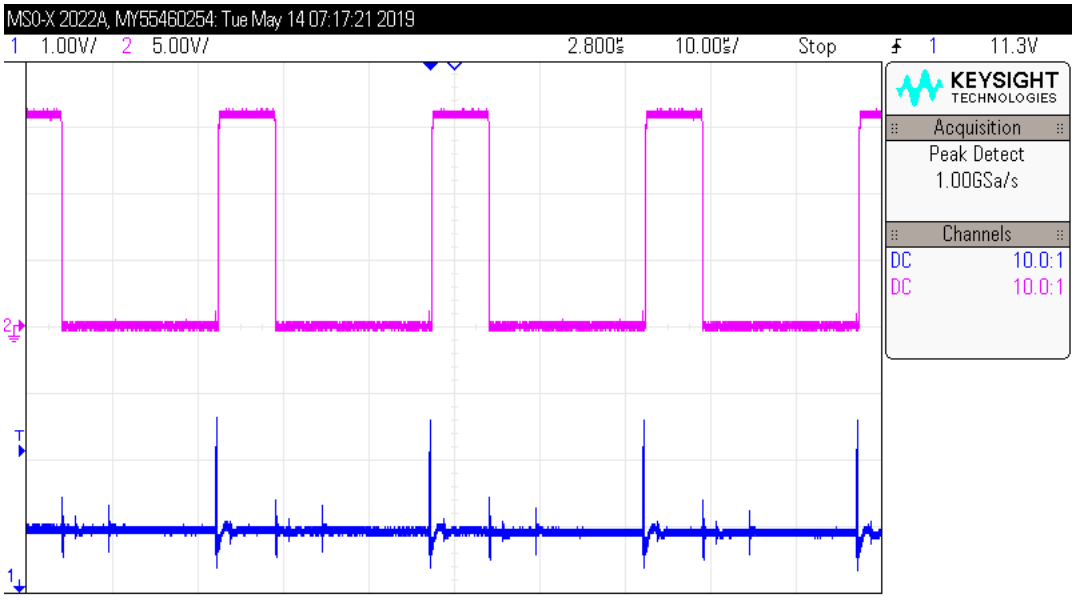

(b)

Figure 58: Trigger Signals Coincide with Switching Noise. (a) I Trigger Signal (Pink) with Distorted Input Signal (Blue). (b) Q Trigger Signal (Pink) with Distorted Input Signal (Blue)

5.5 Transducers Distorting Output Waveform

As mentioned earlier in Section 4.8, another problem that remains unresolved is the ringing of the final SSB-PWM signal upon connecting the transducers to the system. The frequency of the ringing is consistently 8x the fundamental PWM frequency at 320kHz. This is shown in the oscilloscope capture in Figure 59.

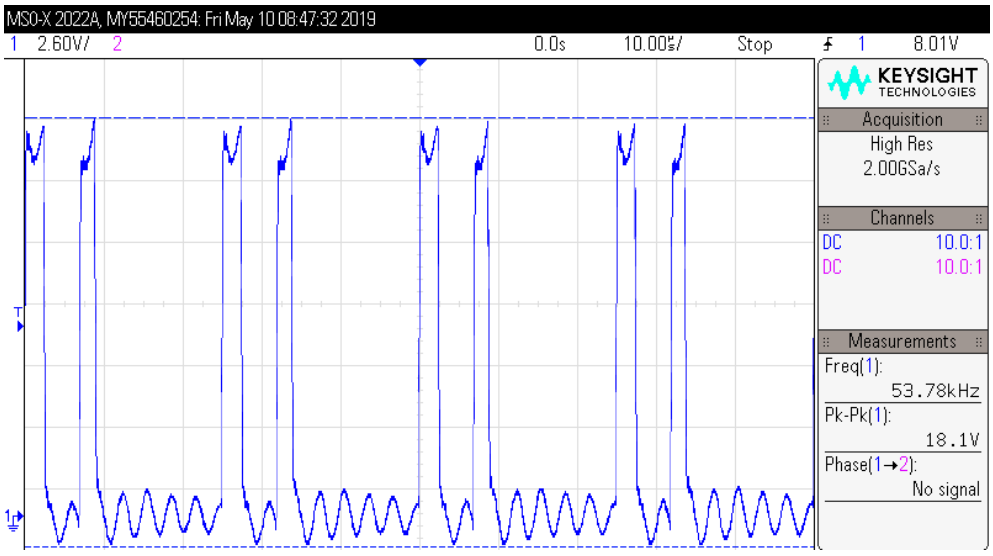

Figure 59: Distorted Output Signal. Harmonic Oscillations Occurring at 320kHz

The exact cause of this ringing is unknown, but it may be related to the MOSFET switching amplifier which is made to drive a capacitive load. If the transducers are not operating at their resonant frequency, there may be some inductance in the load which creates an underdamping effect.

Chapter 6

FUTURE WORK

6.1 Integrator Design Changes

The integrator is designed to attenuate higher frequency signals, but in the current design, these frequencies' voltages are too small to modulate the pulses and produce an audible tone. One possible solution is to increase the supply rail voltage of the op-amp that is used in the integrator, but there is a 1:1 relationship between the supply voltage and the magnitude response. This means offsetting the magnitude response by 20dB would require a 10x increase in the supply voltage. It would not be practical to build a system with components that are rated for over 100V.

Another option would be to employ a partial integration by moving the cutoff frequency higher in the audio spectrum. For example, if the cutoff frequency was chosen to be 2kHz instead of 20Hz, the magnitude response would be flat from 20Hz to 2kHz, and the integration would occur from 2kHz to 20kHz. Figure 60 shows the magnitude response of the partial integration.

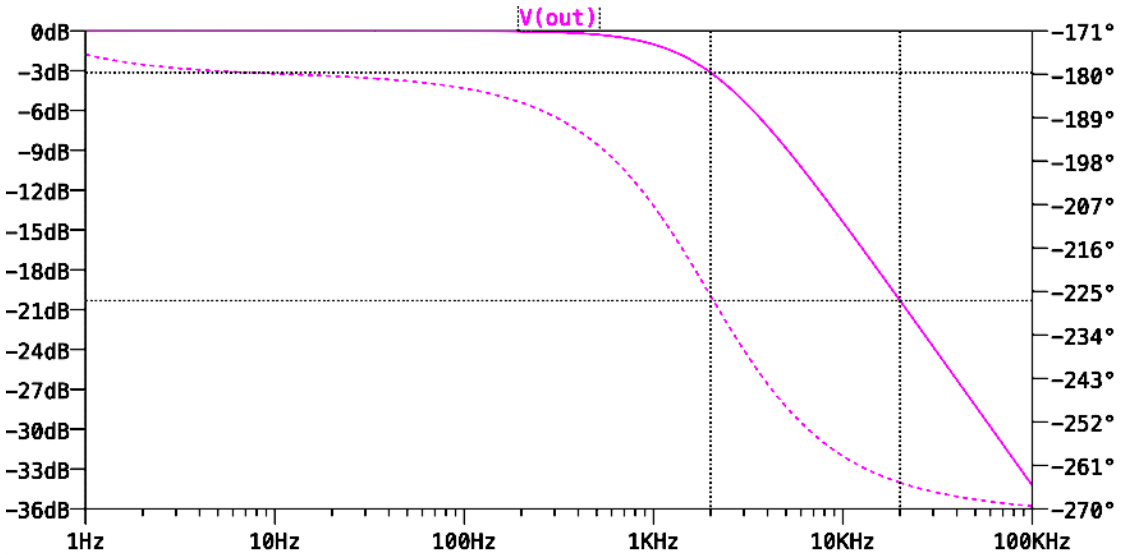

Figure 60: Partial Integration Frequency Response

The benefit of using this integrator design is that the higher frequencies are not nearly as attenuated as before. At 20kHz, the signal is attenuated by -20dB, or 1/10 of the full-scale range, as opposed to 1/1000 of the full-scale range in the original design. Also, the integration is still occurring for a significant portion of the audio spectrum. Out of the 19.98kHz in the audio band, 18kHz is still in the integrating region.

6.2 Reduce Switching Noise in 555 Timers

The exact cause of the switching noise in the timers is unknown. Currently there is a 500nF bypass capacitor close to both timers, but the datasheet of the LM555 timers recommends using a 0.1μF ceramic capacitor and a 1μF electrolytic capacitor per timer. This may help reduce the overall noise on the CV pin.

6.3 Eliminate Harmonic Oscillations in Output Waveform

The 320kHz ringing needs to be removed from the loaded output. A good starting point may be to drive a single transducer directly with a square wave and attempt to replicate the distortion element. Perhaps the transducers have mismatched resonant frequencies that is causing the overall load to have some inductance.

6.4 Improve Transducer Array Design

The transducer array is currently in a square grid pattern in order to maximize the limited space on the perforated board, but for the future there can be a number of improvements to this design. A hexagonal shaped array can ensure that all transducers are equally spaced from one another. This would be best implemented with a custom PCB design with drilled holes that are spaced such that the centers of the transducers are a single diameter away from each other. This will maximize the constructive interference between the ultrasonic waves.

Additionally, a system with more transducers (around 50) driven at a low power may help to reduce THD of the system.

6.5 Hardware Implementation of the Berktay Channel

With a working simulation of the “Berktay Channel” for nonlinear demodulation, a hardware implementation should be possible to create. This would allow for easy testing of various preprocessing schemes in parametric loudspeakers, such as DSB-AM, SRAM, SSB-PWM, etc. to compare the distortion levels of the “demodulated” output. The circuit could be built with an RC Gingell Network, a few multiplier ICs (such as the AD633 [25]) to square the real and imaginary part of the envelope signal, and an op-amp based summing amplifier to combine the two parts and obtain the square of the envelope.

6.6 PCB Based Hardware Design

A PCB based design would greatly improve signal integrity by reducing overall noise in the system and strengthening connections between subcircuits. It would also reduce the physical size of the preprocessor circuit. A dedicated PCB for the transducer array also gives added flexibility; the array can be as large as needed with the appropriate spacing, and the user can aim the ultrasonic beam without moving the rest of the system.

Chapter 7

CONCLUSION

This thesis makes the case for Single Sideband Pulse Width Modulation as a viable preprocessing scheme for parametric loudspeakers. The creation of a PWM based SSB spectrum is accomplished entirely with analog components and ICs. The output circuitry and the transducer array design is where problems arise, preventing comprehensive distortion testing for the hardware. What could not be functionally tested in hardware, tested well in simulation. As shown by the Nonlinear Demodulator, the original signal can be extracted with predictable distortion elements. For future pursuits in this project, more time and resources can be invested in hardware design and implementation. A PCB based design for the processor and the array is a good place to start, and more attention should be given to the transducer array design as well. Perhaps for a better understanding on the wave mechanics side, future work could include consultation with the Physics department or Mechanical Engineering department.

REFERENCES

[1] W. Gan, J. Yang and T. Kamakura, "A review of parametric acoustic array in air", *Applied Acoustics*, vol. 73, no. 12, pp. 1211-1219, 2012. Available: 10.1016/j.apacoust.2012.04.001.

[2] J. Yang, J. Tian and W. Gan, "PARAMETRIC LOUDSPEAKER: FROM THEORY TO APPLICATIONS", in *The 21st International Congress on Sound and Vibration*, Beijing, China, 2019, pp. 1-18.

[3] P. Westervelt, "Parametric Acoustic Array", *The Journal of the Acoustical Society of America*, vol. 35, no. 4, pp. 535-537, 1963. Available: 10.1121/1.1918525 [Accessed 6 June 2019].

[4] H. Berktay, "Possible exploitation of non-linear acoustics in underwater transmitting applications", *Journal of Sound and Vibration*, vol. 2, no. 4, pp. 435-461, 1965. Available: 10.1016/0022-460x(65)90122-7.

[5] C. Shi and W. Gan, "Development of Parametric Loudspeaker", *IEEE Potentials*, vol. 29, no. 6, pp. 20-24, 2010. Available: 10.1109/mpot.2010.938148 [Accessed 7 June 2019].

[6] M. Yoneyama, J. Fujimoto, Y. Kawamo and S. Sasabe, "The audio spotlight: An application of nonlinear interaction of sound waves to a new type of loudspeaker design", *The Journal of the Acoustical Society of America*, vol. 73, no. 5, pp. 1532-1536, 1983. Available: 10.1121/1.389414.

[7] P. Joseph, "Sound from ultrasound: the parametric array as an audible sound source", Ph.D, Massachusetts Institute of Technology, 2002.

[8] S. Sakai, T. Kamakura, B. Enflo, C. Hedberg and L. Kari, "Dynamic single sideband modulation for realizing parametric loudspeaker", *AIP Conference Proceedings*, 2008. Available: 10.1063/1.2956299 [Accessed 6 June 2019].

[9] K. Miura, "Ultrasonic Directive Speaker", *Elektor*, pp. 56-59, 2019.

[10] V. Prodanov, "EE 470 Lecture 21", California Polytechnic State University, 2018.

[11] N. Hay, "COMPLEX FILTERS AS CASCADE OF BUFFERED GINGELL STRUCTURES: DESIGN FROM BAND-PASS CONSTRAINTS", Master's Thesis, California Polytechnic State University, 2017.

[12] K. Choi and H. Liu, “HILBERT TRANSFORM, ANALYTIC SIGNAL, AND SSB MODULATION” *Problem-based learning in communication systems using MATLAB and Simulink*, 1st ed. John Wiley & Sons, Inc., 2016, pp. 109-122.

[13] M. Johansson, "The Hilbert Transform", Master's Thesis, Vaxjo University, 2019.

[14] J. Dugundji, "Envelopes and pre-envelopes of real waveforms", *IEEE Transactions on Information Theory*, vol. 4, no. 1, pp. 53-57, 1958. Available: 10.1109/tit.1958.1057435.

[15] "Monostable Multivibrator using 555 Timer", *Electronics Hub*, 2019. [Online]. Available: https://www.electronicshub.org/monostable-multivibrator-using-555-timer/. [Accessed: 07- Jun- 2019].

[16] "PWM Distortion Analysis | Open Music Labs", *Openmusiclabs.com*, 2019. [Online]. Available: http://www.openmusiclabs.com/learning/digital/pwm-dac/pwm-distortion-analysis/index.html. [Accessed: 07- Jun- 2019].

[17] J. Walling et al., "A Class-E PA With Pulse-Width and Pulse-Position Modulation in 65 nm CMOS", *IEEE Journal of Solid-State Circuits*, vol. 44, no. 6, pp. 1668-1678, 2009. Available: 10.1109/jssc.2009.2020205.

[18] "Network Theory - Series Resonance", *www.tutorialspoint.com*, 2019. [Online]. Available: https://www.tutorialspoint.com/network_theory/network_theory_series_resonance.htm. [Accessed: 07- Jun- 2019].

[19] F. Raab, "Radio Frequency Pulsewidth Modulation", *IEEE Transactions on Communications*, vol. 21, no. 8, pp. 958-966, 1973. Available: 10.1109/tcom.1973.1091763.

[20] MANORSHI ELECTRONICS, “Transmitter Open Type Ultrasonic Probe Black Sensor,” MSO-P1040H07T datasheet.

[21] M. J. Gingell, “Single sideband modulation using sequence asymmetric polyphase networks,” Electrical Commun., vol. 48, no. 1 and 2, 1973.

[22] "Op-Amp Integrator (with Derivation and Solved Examples)", *YouTube*, 2019. [Online]. Available: https://www.youtube.com/watch?v=OPvs7A554Rw. [Accessed: 07- Jun- 2019].

[23] P. Ji, W. Gan, E. Tan and J. Yang, "PERFORMANCE ANALYSIS ON RECURSIVE SINGLE-SIDEBAND AMPLITUDE MODULATION FOR PARAMETRIC LOUDSPEAKERS", Singapore National Research Foundation, Singapore, 2010.

[24] "#215: Basics of crossover distortion | LM358 op amp example", *YouTube*, 2015. [Online]. Available: https://www.youtube.com/watch?v=VgodYtiD_F0. [Accessed: 07- Jun- 2019].

[25] Analog Devices, “Low Cost Analog Multiplier,” AD633 datasheet, Oct. 2002 [Revised Mar. 2015].